Stochastic and reversible assembly of a multiprotein DNA repair complex ensures accurate target site recognition and efficient repair

Martijn S. Luijsterburg,[1,3] Gesa von Bornstaedt,[2,4] Audrey M. Gourdin,[5] Antonio Z. Politi,[6] Martijn J. Moné,[1,3] Daniël O. Warmerdam,[1,5] Joachim Goedhart,[1] Wim Vermeulen,[5] Roel van Driel,[1,3] and Thomas Höfer[2,4]

[1]Swammerdam Institute for Life Sciences, University of Amsterdam, 1098 SM Amsterdam, Netherlands
[2]Research Group Modeling of Biological Systems, German Cancer Research Center, 69120 Heidelberg, Germany
[3]Netherlands Institute for Systems Biology, 1090GE Amsterdam, Netherlands
[4]Bioquant Center, 69120, Heidelberg, Germany
[5]Department of Genetics, Erasmus Medical Center, 3015 GE Rotterdam, Netherlands
[6]Max Delbrück Center for Molecular Medicine, 13092 Berlin-Buch, Germany

To understand how multiprotein complexes assemble and function on chromatin, we combined quantitative analysis of the mammalian nucleotide excision DNA repair (NER) machinery in living cells with computational modeling. We found that individual NER components exchange within tens of seconds between the bound state in repair complexes and the diffusive state in the nucleoplasm, whereas their net accumulation at repair sites evolves over several hours. Based on these in vivo data, we developed a predictive kinetic model for the assembly and function of repair complexes. DNA repair is orchestrated by the interplay of reversible protein-binding events and progressive enzymatic modifications of the chromatin substrate. We demonstrate that faithful recognition of DNA lesions is time consuming, whereas subsequently, repair complexes form rapidly through random and reversible assembly of NER proteins. Our kinetic analysis of the NER system reveals a fundamental conflict between specificity and efficiency of chromatin-associated protein machineries and shows how a trade off is negotiated through reversibility of protein binding.

Introduction

Multiprotein complexes involved in transcription, replication, and DNA repair are assumed to assemble in a sequential and cooperative manner at specific genomic locations (Volker et al., 2001; Black et al., 2006). At the same time, many components of these complexes have been found to exchange rapidly between the chromatin-bound and the freely diffusing protein pools, which has been suggested to serve regulatory functions (Houtsmuller et al., 1999; Dundr et al., 2002; Misteli, 2007; Gorski et al., 2008). We presently do not understand how the ordered formation of chromatin-associated multiprotein machineries can be reconciled with the rapid exchange of their components.

To gain insight into the assembly and functioning of chromatin-associated protein complexes, we have studied the mammalian nucleotide excision repair system, which removes UV-induced DNA damage and other DNA lesions from the genome. Nucleotide excision DNA repair (NER) follows the general organization of chromatin-associated processes, involving: (a) recognition of the target site (e.g., a DNA lesion), (b) assembly of a functional multiprotein complex, and (c) enzymatic action of the machinery on the DNA substrate (Hoeijmakers, 2001; Gillet and Schärer, 2006; Dinant et al., 2009).

M.S. Luijsterburg and G. von Bornstaedt contributed equally to this work.

Correspondence to Roel van Driel: r.vandriel@uva.nl; or Thomas Höfer: t.hoefer@dkfz.de

M.S. Luijsterburg's present address is Dept. of Cell and Molecular Biology, Karolinska Institutet, S-17177 Stockholm, Sweden.

Abbreviations used in this paper: 6-4 PP, 6-4 photoproduct; CPD, cyclobutane pyrimidine dimer; FLIP, fluorescence loss in photobleaching; HU, hydroxyurea; MCMC, Markov chain Monte Carlo; NER, nucleotide excision DNA repair; PCNA, proliferating cell nuclear antigen.

The Rockefeller University Press $30.00
J. Cell Biol. Vol. 189 No. 3   445–463
www.jcb.org/cgi/doi/10.1083/jcb.200909175

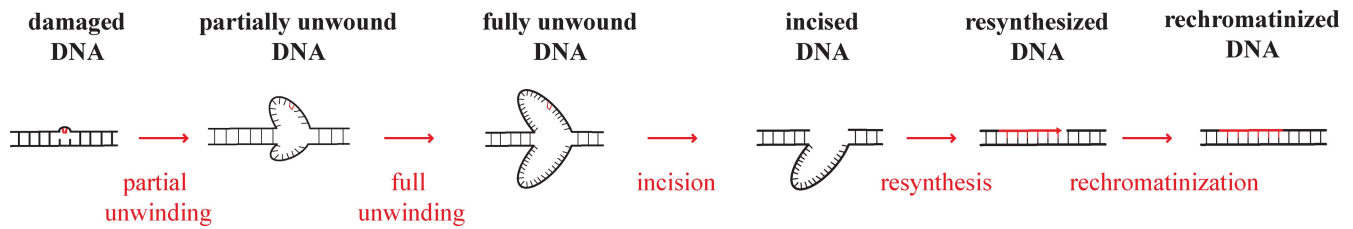JCB   445

THE JOURNAL OF CELL BIOLOGY

Figure 1. **DNA repair intermediates for NER.** The different states of the DNA substrate during NER (repair intermediates) are interconverted by a series of enzymatic reactions (red arrows).

Damage recognition in global genome NER is performed by the XPC-HR23B protein (Sugasawa et al., 1998; Volker et al., 2001). Binding of XPC to lesions triggers the recruitment of TFIIH, which utilizes its helicase activity to locally unwind the DNA around the lesion (Coin et al., 2007; Sugasawa et al., 2009). The unwound DNA is stabilized and acted upon by further proteins: XPA associates with the DNA lesion, RPA binds to the DNA strand opposite to the damage, and the endonucleases XPG and ERCC1/XPF excise ∼30 nucleotides of the unwound DNA strand that contains the lesion (Evans et al., 1997; de Laat et al., 1998; Wakasugi and Sancar, 1999; Park and Choi, 2006; Camenisch et al., 2007). DNA polymerase δ is subsequently loaded by proliferating cell nuclear antigen (PCNA) to fill in the single-stranded gap, which is sealed by the ligase LigIII-XRCCI (Hoeijmakers, 2001; Essers et al., 2005; Moser et al., 2007). Finally, CAF1 assembles new histones on the resynthesized DNA to restore the chromatin structure, completing repair (Green and Almouzni, 2003; Polo et al., 2006).

In vitro studies have been essential in defining the core repair factors and their mode of action but could not account for the dynamic binding of the NER factors to the chromatin substrate (Schaeffer et al., 1993; O'Donovan et al., 1994; Aboussekhra et al., 1995; Sijbers et al., 1996; Riedl et al., 2003; Tapias et al., 2004). In vivo experiments have been crucial in establishing that repair is performed by complexes that are assembled from individual components at the lesion site rather than by binding of a preassembled protein complex (Houtsmuller et al., 1999; Hoogstraten et al., 2002). Together, these studies have led to a conceptual model in which individual NER factors are thought to be incorporated in the chromatin-bound preincision complex in a strict sequential order, followed by the simultaneous dissociation after repair has been completed (Volker et al., 2001; Riedl et al., 2003; Politi et al., 2005). However, previous in vivo studies have focused on the dynamic properties of individual NER proteins and have not addressed the dynamic interplay between NER components during the assembly of the repair complex (Houtsmuller et al., 1999; Hoogstraten et al., 2002; Rademakers et al., 2003; van den Boom et al., 2004; Essers et al., 2005; Zotter et al., 2006; Luijsterburg et al., 2007; Hoogstraten et al., 2008). Thus, a quantitative understanding of how repair complexes assemble in living cells and how the dynamic interactions of NER proteins shape functional properties, such as the rate and specificity of DNA repair, is lacking.

In this study, we present a quantitative analysis of the NER system based on kinetic measurements of seven EGFP-tagged core NER factors in living cells, iterating between experiments and mathematical modeling. We show that all core NER proteins exchange continuously and rapidly on a sub-minute time scale between chromatin-bound and freely diffusing states. In contrast, the repair factors accumulate at repair sites on a much slower time scale, in the order of hours. This paradox is explained by a kinetic model in which repair proteins assemble stochastically and reversibly to form distinct complexes that catalyze the successive enzymatic steps in the NER process, including DNA unwinding, dual incision, and repair synthesis. Notably, a sequential assembly mechanism is incompatible with the experimental data. Although stochastic assembly and disassembly of NER complexes may seem inefficient at first sight, our theoretical analysis shows that this kinetic design realizes a trade off between the conflicting demands of high rate and specificity of DNA repair. Our results indicate that a major determinant of protein affinity, and thus of the composition of NER complexes, is the state of the DNA substrate. Specificity and rate of damage repair emerge as systems properties that depend on the interplay of repair proteins. Our combined approach of live cell imaging experiments and kinetic modeling provides new fundamental insight into the assembly and functioning of a chromatin-associated multiprotein machinery in vivo.

Results

Long-lasting accumulation of NER proteins on damaged DNA

Previous biochemical and in vivo studies of NER have demonstrated that the repair of a DNA lesion proceeds through a series of distinct repair intermediates: damaged, partially unwound, fully unwound, incised, resynthesized, and rechromatinized DNA (Fig. 1; Shivji et al., 1992; Mu et al., 1996; Evans et al., 1997; Tapias et al., 2004; Polo et al., 2006). The interconversion of repair intermediates requires the action of protein complexes with appropriate enzymatic activities that modify the DNA substrate progressively. It has been suggested that individual NER factors assemble into stable repair complexes through a sequential mechanism (Volker et al., 2001; Politi et al., 2005; Mocquet et al., 2008). In this scenario, the individual proteins remain part of the DNA-bound repair complex during the execution of the enzymatic reactions after which they are released. Alternatively, it is possible that repair factors continuously bind to and dissociate from repair complexes while the enzymatic reactions are being performed. In this scenario, the composition of the repair complexes may change in time, such that a series of transient
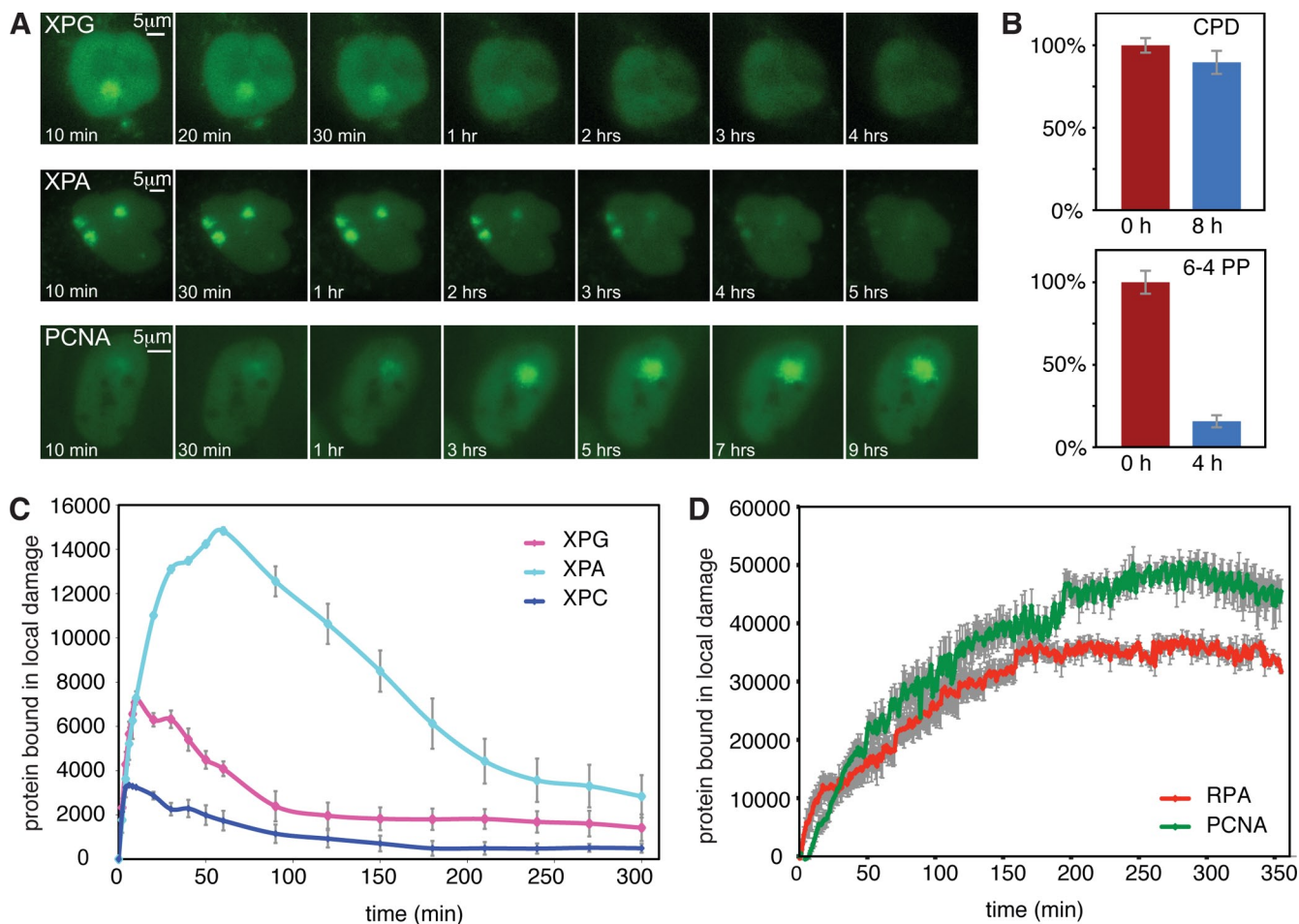
Figure 2. **Long-lasting net accumulation at sites of DNA damage.** (A) Cells stably expressing XPG-EGFP, EGFP-XPA, and EGFP-PCNA shown at various times after local UV-C irradiation (100 J.m^{-2} through 5-µm-diameter pores). (B) Evaluation of the removal of CPDs (top) or 6-4 PPs (bottom) by means of quantitative immunostaining using specific antibodies directly after UV irradiation (0 h) and 4 (for 6-4 PP) or 8 h (for CPD) after UV-C irradiation. Between 50 and 70 cells were analyzed for each time point. (C) Quantification of bound XPC-EGFP (n = 12), XPG-EGFP (n = 5), and EGFP-XPA (n = 7) after UV irradiation. (D) Quantification of bound EGFP-PCNA (n = 5) and RPA-EGFP (n = 5) after UV irradiation. All GFP-tagged repair proteins were stably expressed. (C and D) For consistency, we used only cell nuclei with a single damaged area for quantification. Error bars indicate SEM.

subcomplexes, rather than a single stable complex containing all repair factors, may form at the lesion site.

To analyze the kinetics of the NER process in living cells, we fluorescently tagged seven NER proteins with EGFP and stably expressed the fusion proteins in NER-deficient cells or wild-type cells at physiological levels. The EGFP-tagged NER proteins complement the UV-sensitive phenotype of NER-deficient cells, demonstrating their functionality (see Materials and methods and Fig. S2; Houtsmuller et al., 1999; Hoogstraten et al., 2002, 2008; Rademakers et al., 2003; Essers et al., 2005; Zotter et al., 2006).

We locally irradiated cell nuclei with UV-C light, generating ∼60,000 DNA lesions (6-4 photoproducts [6-4 PPs]) per irradiated area (Fig. S1; Moné et al., 2001). Throughout the repair process, we measured the accumulation kinetics of (a) the lesion recognition factor XPC, (b) components of the preincision complex that excise the lesion (TFIIH, XPG, XPA, and ERCC1/XPF), and (c) proteins involved in the repair synthesis of the generated gap (Fig. 2 A; RPA and PCNA). Accounting for the different nuclear concentrations of the proteins (Table I), we

found that preincision proteins XPA, XPG (the 3′ endonuclease), and RPA accumulated in the damaged area to higher levels than the lesion recognition protein XPC (Fig. 2, C and D). This finding argues against the recruitment of the preincision proteins into a stable NER complex together with XPC at a 1:1 stoichiometry. Moreover, the proteins reached their maximal accumulation at different times, indicating that the composition of NER complexes changes as repair progresses. The protein accumulation seen in the experiments can be attributed to global genome repair rather than transcription-coupled repair, as no recruitment of repair factors XPA, XPG, and RPA is visible upon local UV irradiation in XPC-deficient cells, which can carry out transcription-coupled repair unhindered but have no global genome repair (Volker et al., 2001; Rademakers et al., 2003).

One of the major DNA lesions induced by UV-C irradiation are the 6-4 PPs, which are repaired considerably faster (within ∼5 h) than the cyclobutane pyrimidine dimers (CPDs), which are still present 24 h after UV irradiation (van Hoffen et al., 1995). During the time span of 6-4 PP repair, in which we

Table I. **Values of binding and dissociation rate constants**

Value	XPC	TFIIH	XPG	XPA	XPF/ ERCC1	RPA	PCNA
Concentration (µM)	0.140	0.360	0.440	1.110	0.170	1.110	1.110
Damaged DNA							
k_{on} (µM^{-1}s^{-1})	0.008 (0.007; 0.011)	1.6 (0.8; 4.5)	NA	NA	NA	NA	NA
k_{off} (s^{-1})	0.061 (0.007; 0.462)	0.053 (0.004; 0.195)	NA	NA	NA	NA	NA
K_d (µM)	7.8	0.03	NA	NA	NA	NA	NA
Partially unwound DNA							
k_{on} (µM^{-1}s^{-1})	0.002 (0.001; 0.003)	0.26 (0.11; 0.27)	0.28 (0.19; 0.31)	0.13 (0.12; 0.16)	1.2 (1.1; 1.6)	0.15 (0.11; 0.22)	NA
k_{off} (s^{-1})	0.007 (0.006; 0.008)	0.012 (0.009; 0.016)	0.015 (0.012; 0.015)	1.04 (0.75; 1.30)	0.01 (0.011; 0.014)	2.6 (1.7; 3.6)	NA
K_d (µM)	3.1	0.05	0.05	7.7	0.01	17	NA
$\tau = 35 \pm 30$ min							
Fully unwound DNA							
k_{on} (µM^{-1}s^{-1})	0.002 (0.001; 0.003)	0.26 (0.11; 0.27)	0.28 (0.19; 0.31)	0.13 (0.12; 0.16)	1.2 (1.1; 1.6)	0.006 (0.006; 0.007)	NA
k_{off} (s^{-1})	0.007 (0.006; 0.008)	0.012 (0.009; 0.016)	0.015 (0.012; 0.015)	1.04 (0.75; 1.30)	0.01 (0.011; 0.014)	0.021 (0.020; 0.022)	NA
K_d (µM)	3.1	0.05	0.05	7.7	0.01	3.27	NA
$\tau = 41 \pm 36$ min							
Incised DNA							
k_{on} (µM^{-1}s^{-1})	0.22 (0.13; 0.26)	0.0004 (0.0003; 0.010)	0.001 (0.0004; 0.007)	0.004 (0.004; 0.005)	0.09 (0.07; 0.11)	0.006 (0.006; 0.007)	0.001 (0.001; 0.002)
k_{off} (s^{-1})	0.40 (0.21; 0.48)	0.05 (0.04; 0.07)	0.10 (0.04; 0.11)	0.06 (0.05; 0.07)	0.050 (0.040; 0.101)	0.021 (0.020; 0.022)	0.004 (0.004; 0.004)
K_d (µM)	1.8	137	89	13	0.53	3.27	2.8
$\tau = 41 \pm 36$ min							
Resynthesized DNA							
k_{on} (µM^{-1}s^{-1})	NA	NA	NA	0.054 (0.054; 0.058)	NA	0.08 (0.05; 0.10)	0.010 (0.007; 0.010)
k_{off} (s^{-1})	NA	NA	NA	0.004 (0.004; 0.005)	NA	0.04 (0.03; 0.05)	0.002 (0.002; 0.002)
K_d (µM)	NA	NA	NA	0.08	NA	0.51	0.19
$\tau = 2.0 \pm 0.7$ h							
Rechromatinized DNA							
k_{on} (µM^{-1}s^{-1})	NA	NA	NA	NA	NA	0.07 (0.06; 0.07)	0.31 (0.25; 0.34)
k_{off} (s^{-1})	NA	NA	NA	NA	NA	0.04 (0.04; 0.05)	0.05 (0.04; 0.05)
K_d (µM)	NA	NA	NA	NA	NA	0.61	0.16
$\tau = 2.2 \pm 0.7$ h							

NA, not applicable. The values for the different repair proteins are arranged in columns for the different DNA repair intermediates to which they bind (rows). The dissociation constants $K_d = k_{off}/k_{on}$ are also given. Reference parameter set and 90% confidence intervals (in parentheses) are shown. Nuclear concentration (in micromolars) of NER factors XPC, XPA, and XPG are based on previously described data (Araújo et al., 2001), whereas RPA and PCNA amounts are estimated to be 250,000 molecules per cell, and TFIIH and ERCC1-XPF were estimated at 65,000 and 50,000 molecules per cell, respectively, based on previous estimates (Houtsmuller et al., 1999; Moné et al., 2004). Concentrations are calculated assuming a nuclear volume of 0.3 pL.

confirmed CPD repair to be negligible (Fig. 2 B), the degree of accumulation of the different NER factors declined at different rates. After reaching a maximum, bound XPC- and XPG-EGFP levels gradually decreased with a $t_{1/2}$ of ~1 h (Fig. 2 C), which is similar to the decrease in bound ERCC1-GFP (Politi et al., 2005). Bound EGFP-XPA decreased more slowly ($t_{1/2}$ ~2.5 h; Fig. 2 C), whereas EGFP-PCNA and RPA-EGFP did not decrease within 5 h after UV-C irradiation (Fig. 2 D). For the analysis of RPA and PCNA, we selected cells that were not undergoing S phase to assure that binding of these proteins is not the result of DNA replication. These repair synthesis proteins also accumulated at sites of DNA damage in quiescent cells (unpublished data), further confirming that the binding reflects engagement in DNA repair and not DNA replication.

These results show that NER proteins are engaged in repair for several hours. The mean molecular composition of the NER complexes changes as DNA repair progresses: the damage recognition factor XPC and the two endonucleases XPG and ERCC1/ XPF reach their maximal accumulation level early (~10 min after irradiation), XPA displays intermediate behavior (~1 h), and the accumulation of PCNA and RPA is considerably slower (maximum at ~4 h) and lasts longer.

Rapid exchange of NER proteins

Our measurements of the net accumulation kinetics are compatible both with the stable recruitment of repair factors into long-lived complexes and with a scenario in which repair factors associate with and dissociate from repair complexes continuously while repair of a lesion is being performed. To distinguish between these different mechanisms, we measured the dwell times of the NER proteins at sites of DNA damage using fluorescence loss in photobleaching (FLIP; see Materials and methods). In brief, a region distant from the repair site was continuously bleached at 100% laser power, whereas the decrease of fluorescence in the locally damaged area was measured at low laser intensity. We chose experimental conditions in which an EGFP-tagged repair protein that dissociates from sites of DNA damage has a high probability to be bleached before rebinding to a site of damage (see Materials and methods). To determine the contribution of diffusion, we compared the FLIP kinetics of proteins accumulated in the damaged area and of proteins outside the irradiated area at a similar distance from the bleaching area. FLIP kinetics for the latter were at least one order of magnitude faster, implying that binding, but not diffusion, is rate limiting for the dwell time of the NER proteins in the damaged area (unpublished data). Monitoring the loss of accumulated NER factors in the damaged region, we found that all EGFP-tagged preincision proteins dissociated rapidly from repair complexes, with overall half-lives of 20 (RPA), 25 (XPC), 50 (TFIIH, XPG, and ERCC1/XPF), and 80 s (XPA; Fig. 3, A and B). The dissociation kinetics of the repair synthesis factor PCNA were strongly biphasic, with half-lives of 10 and 225 s for the two components (Fig. 3, A and C). Conversely, when monitoring EGFP-tagged histone H4 outside the bleaching area, we did not detect any loss in fluorescence, as would be expected for an immobile component of chromatin (Fig. 3, A and B; Kimura and Cook, 2001). Control experiments showed that cells analyzed by FLIP were still fully capable of repairing UV-induced DNA lesions (Fig. S3), indicating that the FLIP procedure does not affect the repair capacity of a cell.

To verify the FLIP results, we conducted complementary photoconversion experiments using mOrange (Kremers et al., 2009). Monitoring the loss of photoconverted XPC-mOrange or mOrange-XPA in the damaged region confirmed that these NER proteins dissociate rapidly from repair complexes (half-lives of ∼25 and 80 s; Fig. 4, A, B, and D). Likewise, bleaching the entire nucleus except for the local accumulation of XPC-mOrange or mOrange-XPA and measuring the loss of fluorescence in the local damage (inverse FRAP; Dundr et al., 2002) gave very similar dissociation curves as FLIP and photoconversion experiments (Fig. 4, C and E). Thus, all measured NER factors exchange rapidly between the freely diffusing and bound states, being part of a repair complex on average for a few tens of seconds. This rapid exchange of individual proteins strongly contrasts with the long overall persistence of repair complexes at UV-damaged sites.

We then perturbed the repair process and measured how this affects the dwell times of NER proteins. When NER was blocked before lesion excision, either by impaired unwinding in cells lacking functional XPB, XPA, or XPG or by impaired excision in cells with compromised ERCC1 or XPF (Evans et al., 1997), XPC dissociation was about fourfold slower than in wild-type cells. This suggests that XPC is bound more stably before dual incision has occurred (irrespective of whether other NER factors can bind or not bind when DNA unwinding is impaired; Fig. 3 D). The observation of prolonged accumulation of XPA during NER prompted us to investigate whether XPA remains bound after dual incision has occurred. To stall NER at the repair synthesis stage, we added hydroxyurea (HU) and AraC (cytosine–β-arabinofuranoside), which are inhibitors of repair synthesis and DNA ligation (Smith and Okumoto, 1984; Mullenders et al., 1987), respectively, ∼1 h before local UV-C irradiation. Subsequently, the cells were locally irradiated, and we measured the dwell times of repair factors by FLIP. Blocking repair synthesis and ligation affected the dissociation of XPA and PCNA (Fig. 3, C and E). XPA dissociation was about twofold faster if DNA synthesis and ligation was inhibited, showing that XPA binds to repair synthesis intermediates with high affinity. Dissociation of PCNA was slower in the presence of HU and AraC, indicating its preferential binding to incised DNA (Shivji et al., 1995). The same treatment had no effect on the dissociation kinetics of XPC and ERCC1/XPF (Fig. 3 E). Thus, in contrast to the other preincision proteins, XPA binding becomes stabilized in the process of repair synthesis. These results show that the dwell times of NER proteins change as repair progresses and suggest that the state of the DNA substrate is an important determinant of protein affinity.

Random and rapidly reversible assembly of functional NER complexes

The experiments show kinetics of all proteins involved in NER on two very different time scales. The slow (hours) net accumulation and release of NER proteins at damaged nuclear areas contrasts with their rapid (subminute) exchange between chromatin-bound and unbound states.

To rationalize the experimental findings, we developed a mathematical model of NER. The scaffold of the model is formed by the sequence of enzymatic reaction steps carrying out DNA unwinding, dual incision, and repair synthesis. We assume that DNA adjacent to the lesion is unwound in two steps (Evans et al., 1997) and thus distinguish six DNA repair intermediates (Fig. 1). We have extracted from our work and the work of others the composition of the enzymatically active multiprotein complexes that catalyze the transitions between the repair intermediates (Fig. 5 A and Table S1). Specifically, DNA lesions are recognized by XPC, and the subsequent binding of TFIIH causes unwinding of the DNA around the lesion (Sugasawa et al., 2009). Upon DNA unwinding, all repair proteins can bind to and dissociate from the repair intermediates in any order. Completely sequential and random assembly mechanisms are the extremes of a spectrum of potential assembly mechanisms that the model can describe (Fig. 5 B).

Because the mathematical model distinguishes between enzymatic reactions that interconvert the repair intermediates and the association/dissociation steps of the individual repair proteins, it allows us to scrutinize potential NER complex assembly mechanisms from the in vivo measurements of the core
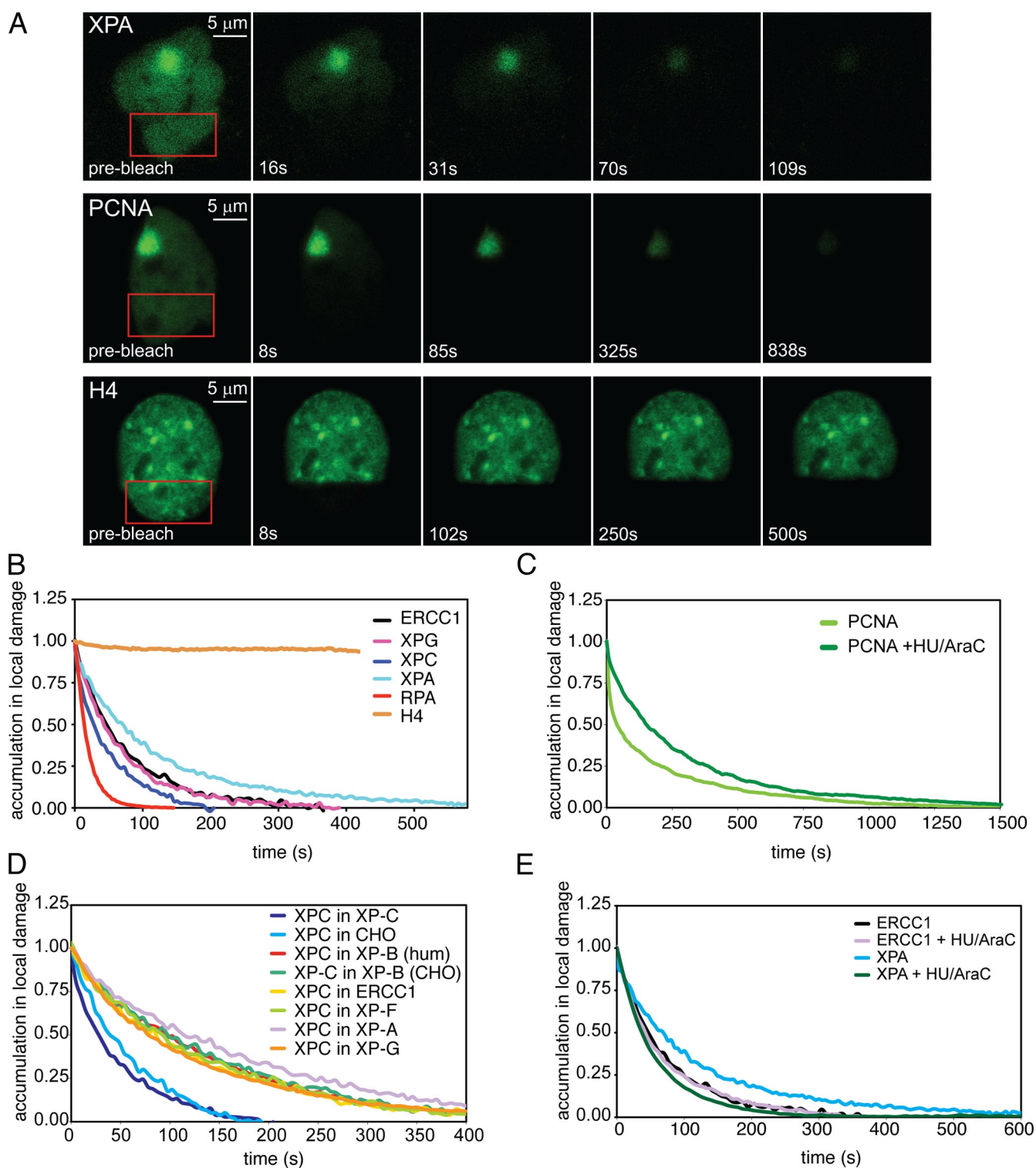
Figure 3. **Rapid exchange of NER proteins at sites of DNA damage.** (A) FLIP measurements in XP2OS cells stably expressing EGFP-XPA (1 h after damage), CHO9 cells stably expressing EGFP-PCNA (2 h after damage), and MRC5 cells transiently expressing EGFP–histone H4. The cells were continuously bleached in the undamaged region (red rectangles), and loss of fluorescence was monitored with low laser intensity in the locally damaged area. (B) Quantification of FLIP experiments on XPC-EGFP in XPC-deficient XP4PA cells, XPG-EGFP in XPG/ERCC5-deficient UV135 cells, EGFP-XPA in XPA-deficient XP2OS cells, RPA-EGFP in MRC5 cells, ERCC1-GFP in ERCC1-deficient 43-3B cells, and EGFP-H4 in MRC5 cells. (C) Quantification of FLIP experiments on EGFP-PCNA in CHO9 cells. All GFP-tagged repair proteins were stably expressed. GFP-H4 was transiently expressed. (D) Quantification of FLIP experiments with perturbations of NER on XPC-mVenus transiently expressed at low levels in various locally irradiated NER-deficient CHO and human cell lines. The following NER mutant cell lines were used: CHO XP-B/ERCC3–deficient 27.1 cells, XPG/ERCC5-deficient UV135 cells and ERCC1-deficient 43-3B cells, and human XPB–deficient XPCS2BA-SV cells (Vermeulen et al., 1994), XPA-deficient XP12RO-SV cells and XPF-deficient XP2YO-SV cells. Additionally, XPC-mVenus was also transiently expressed in wild-type CHO-K1 cells. (E) Quantification of FLIP experiments in the absence or presence of HU and AraC on locally irradiated XP2OS cells expressing stably EGFP-XPA or 43-3B cells stably expressing ERCC1-GFP. The kinetics of EGFP-PCNA in the presence of HU and AraC are shown in C.
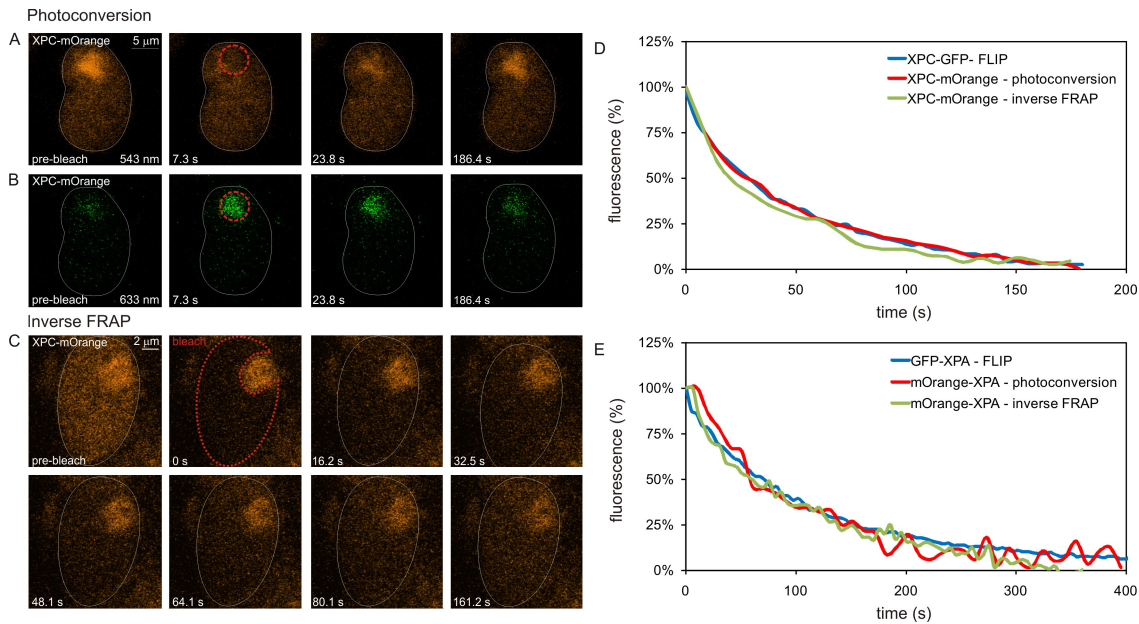
Figure 4. Photoconversion and inverse FRAP on NER proteins XPC and XPA in the damaged area. Example of a photoconversion experiment on XP4PA cells transiently expressing low levels of XPC-mOrange. (A and B) Cells were locally irradiated (5 μm; 100 J.m^{-2}) and monitored in the orange channel (A; 543 nm; nonphotoconverted) and the far-red channel (B; 633 nm; photoconverted). 30 min after local UV irradiation, the local accumulation of XPC-mOrange was photoconverted with 488-nm laser light. The levels of nonphotoconverted XPC-mOrange increased at the local damage site (A), whereas the levels of photoconverted XPC-mOrange decreased as a result of the rapid exchange of XPC at the damaged site (B). (B) Example of an inverse FRAP experiment on XP4PA cells transiently expressing low levels of XPC-mOrange. Cells were locally irradiated (5 μm; 100 J.m^{-2}). (C) 30 min after local UV irradiation, the entire nucleus except for the local accumulation of XPC-mOrange at the damaged area was bleached (the bleach region is indicated in red). Cells were monitored in time until the ratio between the fluorescence intensity in the local damage and in the nucleoplasm were restored to the prebleach value. (D) Quantification of the dwell time of XPC-mOrange as measured by photoconversion (red) and inverse FRAP (green). The blue curve, which shows the dwell time of XPC-EGFP measured by FLIP (Fig. 3 B), is shown for comparison. (E) Quantification of the dwell time of mOrange-XPA as measured by photoconversion (red) and inverse FRAP (green). The blue curve, which shows the dwell time of EGFP-XPA as measured by FLIP (Fig. 3 B), is shown for comparison.

NER factors. We found that a strict order of protein binding to the repair intermediates (sequential assembly) would imply the stabilization of early binding proteins by the subsequent proteins incorporated into the complex, resulting in long dwell times of early-binding proteins compared with short dwell times of late-binding proteins. Thus, the recruitment of proteins in a strict order is incompatible with the mutually independent and rapid dissociation of individual NER factors that we observe. In contrast, a random binding and dissociation mechanism of repair proteins can account for both rapid exchange and slow net accumulation of NER proteins at sites of damage, as follows.

We model the formation of multiprotein complexes at the DNA lesions as a predominantly stochastic process in which proteins can associate and dissociate independently of each other and in any order as soon as the DNA becomes partially unwound. When an enzymatically active protein complex is assembled (e.g., the preincision complex with the two endonucleases XPG and ERCC1/XPF), it catalyzes the transition from one DNA repair intermediate to the next (e.g., the excision of the damaged region). Thus, the modeling framework accounts for reversible protein binding as well as irreversible enzymatic reactions that determine the directionality of NER (Fig. 5 A). This model translates into a system of differential equations for the various protein complexes formed at the DNA repair intermediates (Fig. 5 B).

We derived k_{on} and k_{off} values for the binding of the individual proteins to the different repair intermediates and k_{cat} values for the enzymatic reactions by fitting the model to the experimental data (see Materials and methods). For this purpose, we implemented a Markov chain Monte Carlo (MCMC) method to systematically explore the parameter space (ranges for the k_{on}, k_{off}, and k_{cat} values) and obtained a model fit that reproduces all available experimental data simultaneously, including the net accumulation kinetics, the FLIP kinetics for normal NER, and NER blocked at different stages (Fig. 6, A–D). The MCMC algorithm for deriving kinetic parameters from the experimental data also yielded confidence intervals for the estimated parameters (Tables I and II).

Thus, the computational analysis shows that the comprehensive experimental dataset for kinetics of the core NER factors is consistent with a rapidly reversible and predominantly random assembly mechanism of NER complexes.

Lesion recognition is rate limiting for NER

All kinetic parameters extracted from the experimental data fall in biochemically realistic ranges. The in vivo affinities of the NER proteins for the repair intermediates span a considerable range, from micromolar to nanomolar values for the dissociation constants ($K_d = k_{off}/k_{on}$; Fig. 6 E). The model also yields the time evolution of the six DNA repair intermediates (Fig. 6 F). DNA lesions are excised on average 41 ± 36 min after UV irradiation,
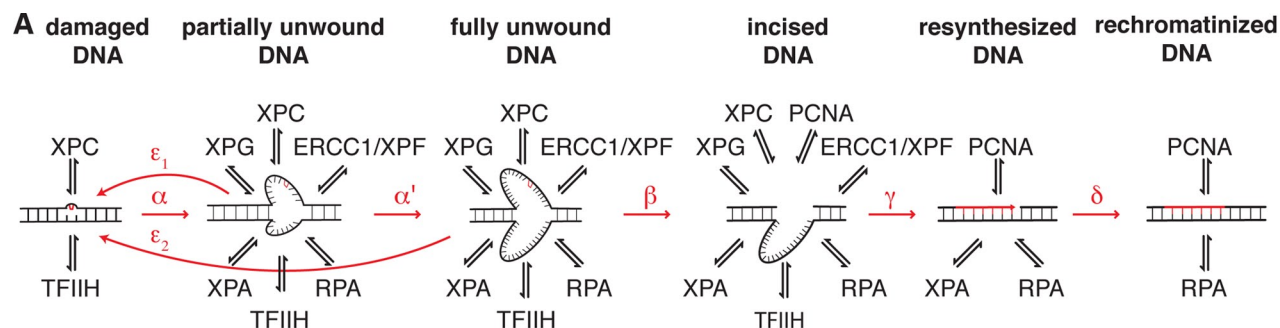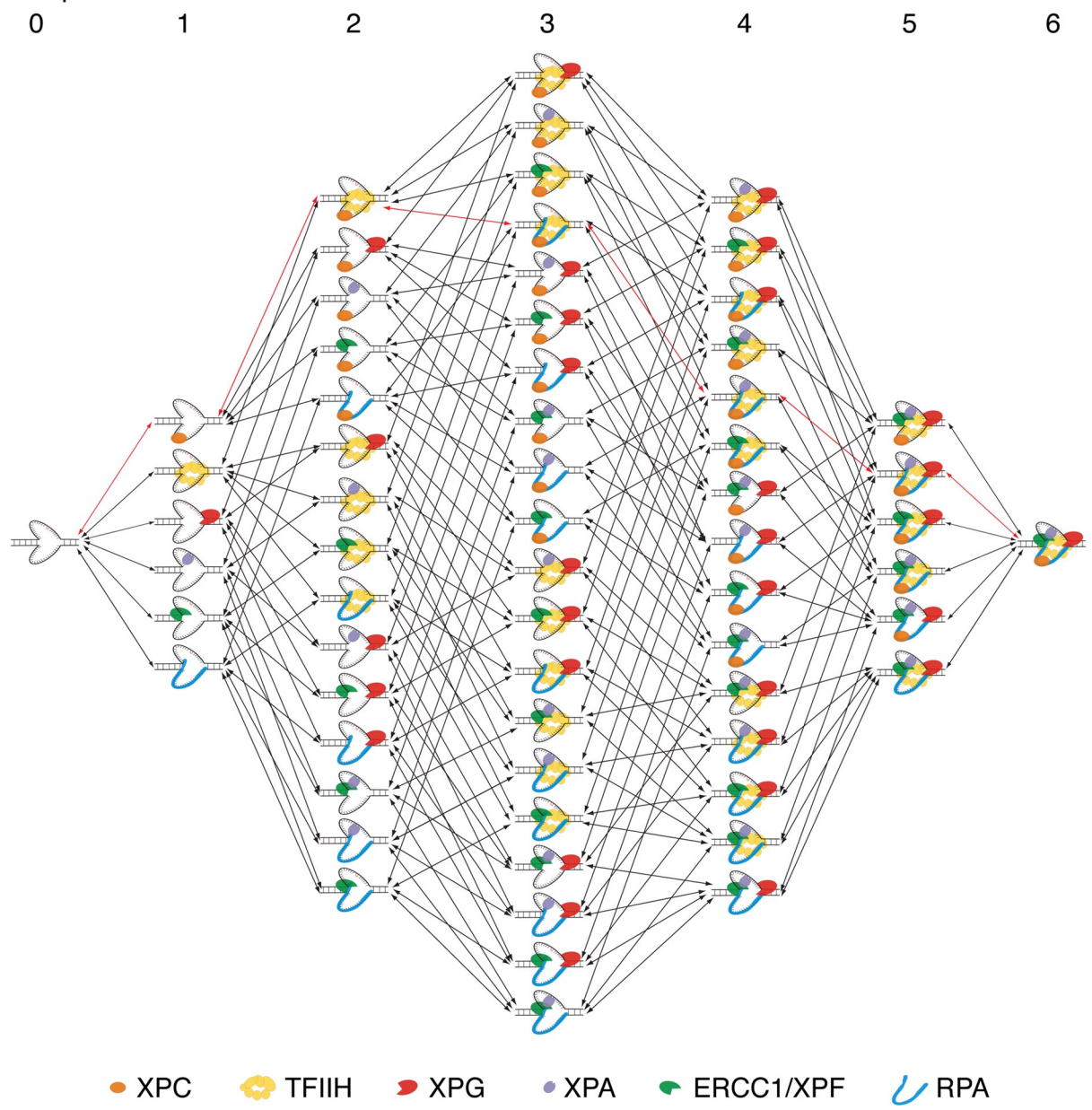
Figure 5. **Kinetic model of NER.** The model distinguishes six DNA repair intermediates, as indicated, that are interconverted by enzymatic steps. Red arrows: α, partial DNA unwinding; α', full unwinding; β, dual incision; γ, resynthesis; δ, rechromatinization; ε_1 and ε_2, reannealing of unwound DNA when it becomes devoid of stabilizing proteins. The indicated NER proteins can bind to the repair intermediates. The binding of TFIIH to the DNA lesion requires the prior binding of XPC. The binding of XPA and ERCC1/XPF is cooperative (Table S1). (B) Possible assembly pathways for the preincision complex on unwound DNA. Random assembly can use all pathways shown, whereas sequential assembly will follow a unique pathway (e.g., the pathway indicated by the red arrows assuming ordered binding of XPC, TFIIH, RPA, XPA, XPG, and ERCC1/XPF).
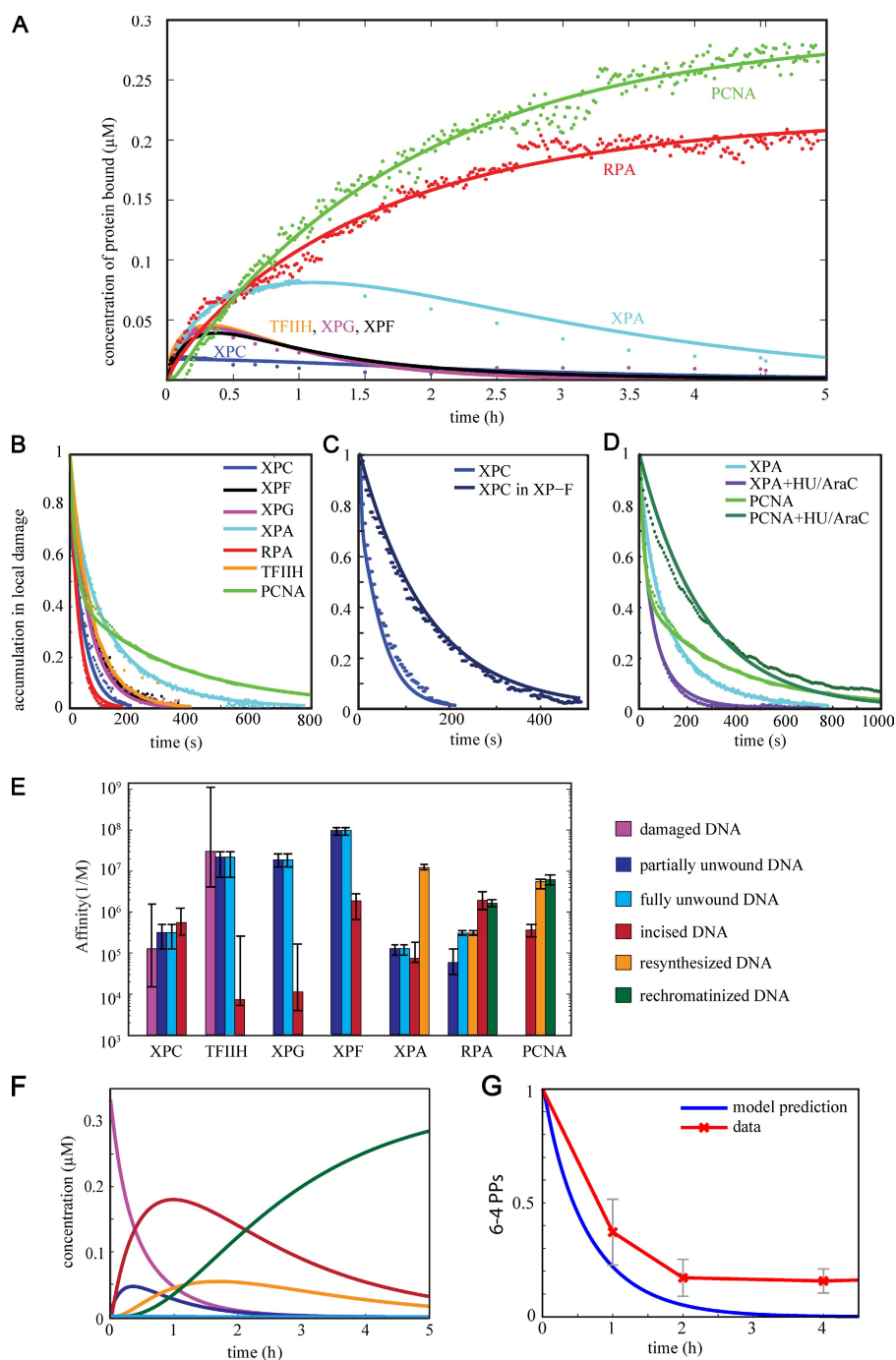
Figure 6. **Random and reversible NER complex assembly accounts both for rapid exchange and prolonged net accumulation of repair proteins.** (A–D) Comparison of model simulations (lines) and experimental data (dots) showing net accumulation kinetics (A) and dissociation kinetics (B) of core NER proteins, dissociation kinetics of XPC in wild-type and XPF-deficient cells unable to perform damage excision (C), and dissociation kinetics of XPA and PCNA in the absence or presence of DNA synthesis/ligation inhibitors HU and AraC (D). (E) Affinity of NER proteins for the repair intermediates ($K_a = k_{on}/k_{off}$). Preincision factors XPG, TFIIH, and ERCC1/XPF lose affinity after lesion excision, whereas the affinities of XPA, PCNA, and RPA increase upon repair synthesis. (F) Computed time courses of the repair intermediates. Note that the color coding of the repair intermediates, as indicated in E, also applies to F. (G) Comparison between the predicted kinetics of the removal of 6-4 PPs (blue) and the measurements on the kinetics of 6-4 PP removal by means of quantitative immunostaining using specific antibodies (red). Between 50 and 70 cells were analyzed for each time point. Error bars indicate SD.

with large stochastic variation from lesion to lesion (see Materials and methods). Damage recognition by XPC and partial unwinding of the DNA by TFIIH takes on average ∼35 min, and subsequently, ∼6 min are sufficient to fully unwind the DNA and assemble the preincision complex containing XPA, XPG, ERCC1/XPF, RPA, and TFIIH. Thus, the incision time is mainly determined by slow lesion recognition through XPC, after which a functional preincision complex is rapidly formed through random assembly. In agreement, we find that the preincision factors assemble with similar initial rates on chromatin (∼15 molecules/s; Fig. 2, C and D; and Fig. S4 A). Indeed, we found that the existence of many different assembly routes in the random mechanisms

(Fig. 5 B) outweighs the disadvantage of creating a large number of partially assembled complexes and allows rapid complex assembly (not depicted).

To validate the predicted repair kinetics, we experimentally measured the removal of DNA lesions (6-4 PPs) by quantitative immunostaining (see Materials and methods). The experimentally measured kinetics of lesion excision indeed occurred on the time scale predicted by the model, which was considerably slower (tens of minutes to hours) than the dwell time of individual repair factors (seconds to minutes; Fig. 6 G).

To summarize, the model indicates that recognition of a DNA lesion is time consuming, whereas subsequent preincision

Figure 7. **Capacity of NER.** (A) Control of NER proteins on the rate of incision (black) and rate of DNA resynthesis (gray). Control coefficients were calculated with the following equation:

$$C_i^\tau = \frac{X_i}{\tau^{-1}} \frac{\partial \tau^{-1}}{\partial X},$$

where τ denotes the mean time (for incision or repair synthesis) and X_i the total concentration of protein i. (B) The model correctly predicts the kinetics of XPG binding when the amount of initial DNA damage is increased $\sim$2.6-fold (+, experimental data for irradiation through 8-µm pores; red line, model simulation) as compared with reference conditions (x, experimental data; blue line, model). (C) Maximally bound XPG-EGFP after local UV-C irradiation of differently sized areas (100 J.m^{-2} through 3-, 5-, and 8-µm pores). (D) The model correctly predicts the kinetics (amplitude and shape of the curve) of XPC-EGFP binding in XPA-deficient cells (red line, model prediction; red crosses, experimental data). The predicted curve and the measured kinetics of XPC-EGFP binding in (complemented) XPC-deficient cells are shown in blue for comparison. Error bars indicate SD.
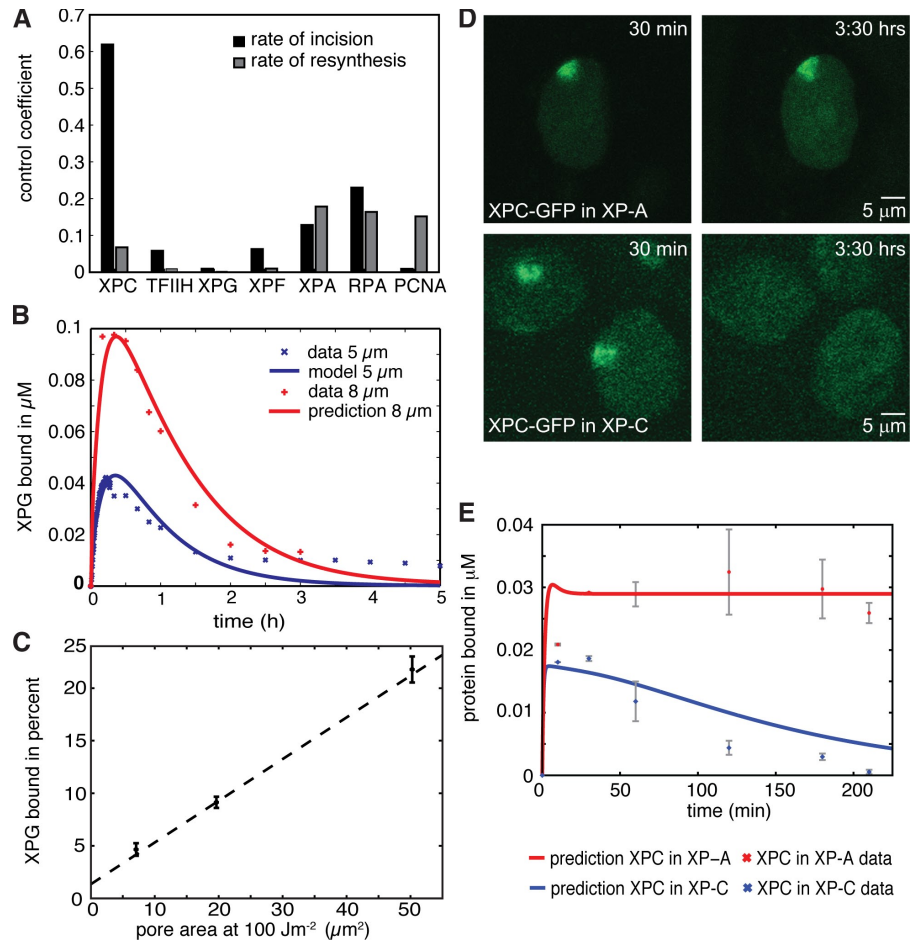
High capacity for parallel processing of DNA lesions

To determine the control of each NER protein on the rates of incision and repair synthesis, we calculated the control coefficients that quantify how a change in the concentration of an individual protein affects these rates (Materials and methods). Most proteins have an appreciable impact, showing that the rate of NER is a systems property rather than being determined by a single protein (Fig. 7 A). However, XPC has the dominant control on the rate of incision, whereas RPA, XPA, and PCNA control the rate of repair synthesis.

To quantify the dependence of the rate (v) of NER on the amount of DNA lesions (D), we approximated the repair rate by the Michaelis–Menten equation $v = v_{max} D/(K_M + D)$. From our data, we estimated the maximal rate $v_{max} = 6{,}000$ lesions min^{-1} (see Materials and methods), which agrees with previous measurements (Kaufmann and Wilson, 1990; Ye et al., 1999). The estimated half-saturation at $K_M = 216{,}000$ lesions indicates that NER is not saturated under our experimental conditions ($\sim$60,000 DNA lesions at $t = 0$). In fact, the model predicts that an increase in the number of DNA lesions would not change the net accumulation kinetics of a repair factor. Rather, it would

increase the number of repair proteins engaged in DNA repair (Fig. 7 B, red line), and this increase in engaged DNA repair proteins is predicted to be approximately proportional to the number of DNA lesions.

To address experimentally whether NER is indeed unsaturated, we inflicted different amounts of DNA damage per nucleus and monitored the accumulation of the preincision protein XPG. The experimental curves for the measured amplitude and kinetics of XPG accumulation for increased DNA damage matched the predicted curves generated by the model (Fig. 7 B, red crosses). Nearly twice the number of XPG molecules was engaged in DNA repair when the number of DNA lesions was doubled, without changes in the long-term accumulation of XPG, which fully agreed with the model prediction (Fig. 7 B). Further supporting the prediction that NER is far from saturation, we observed an essentially linear relationship between XPG accumulation and the number of DNA lesions (Fig. 7 C and Fig. S4 B). Thus, NER has a high capacity to process DNA lesions in parallel.

As global genome NER is strictly dependent on damage recognition by XPC (Volker et al., 2001), we further tested to what extent XPC ($\sim$0.14 µM) can become bound to DNA damage (6-4 PP; $\sim$0.33 µM). When the repair of the DNA lesions is prevented, the model predicts only a moderate increase in XPC net accumulation because of the rather low XPC affinity (Fig. 7 E, red line, compare with blue line for predicted XPC
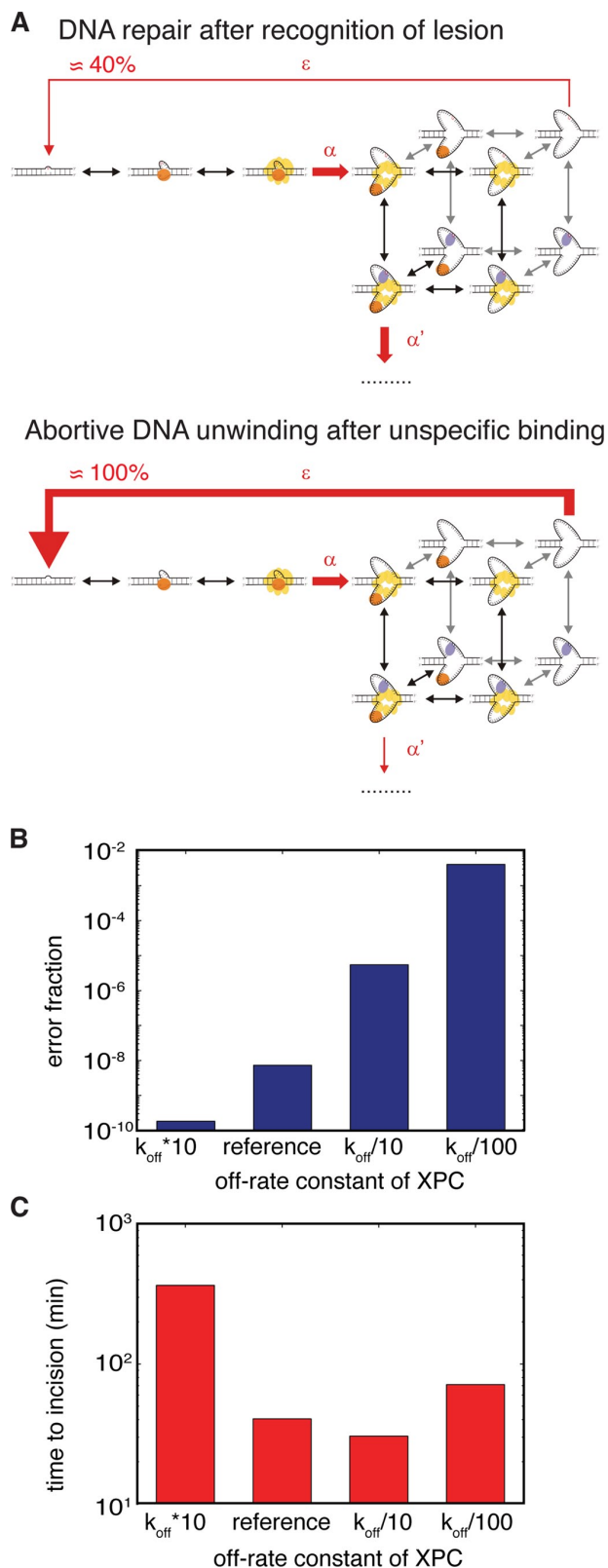
A DNA repair after recognition of lesion

Abortive DNA unwinding after unspecific binding

B

C

accumulation when repair takes place). To test this prediction, we expressed XPC-EGFP in repair-deficient XP-A cells and measured its binding kinetics after localized UV irradiation (Fig. 7 D). The net accumulation of XPC-EGFP on DNA damage in XPA-deficient cells was indeed only slightly increased compared with its accumulation in repair-proficient cells and closely matched the amplitude predicted by the model (Fig. 7 E, red crosses and red line, respectively). Unlike the decreasing XPC accumulation in repair-proficient cells (Fig. 7, D and E, blue crosses), XPC accumulation in the repair-deficient cells remained at a plateau level in further agreement with the model prediction. Remarkably, this plateau is at ∼10% of the estimated total DNA damages (6-4 PPs). This finding corroborates the prediction of low XPC affinity and indicates that the unsaturated nature of NER is, at least in part, due to the comparatively weak XPC binding.

Reversible binding of repair proteins can ensure accurate damage recognition

The NER machinery must recognize DNA lesions with high specificity to avoid accidental repair of nondamaged DNA, which is potentially mutagenic. The lesion recognition factor XPC binds to DNA damage with only ∼100-fold higher affinity than to undamaged DNA (Hey et al., 2002; Hoogstraten et al., 2008). About 10^5 incisions on nondamaged sites per hour would occur if the specificity of NER were determined by XPC alone (see Materials and methods). Obviously, much higher damage specificity is required to prevent erroneous DNA incisions by the NER machinery. The model demonstrates that specificity can be increased by several orders of magnitude through a kinetic proofreading mechanism based on the reversibility of DNA unwinding. Using model simulations, we estimate that most DNA unwinding events around a true lesion immediately lead to incision (∼60%). In the remaining cases, DNA reanneals before a preincision complex is formed and NER starts again by XPC binding to the lesion. In contrast, XPC and other NER factors bind so weakly in the absence of a lesion that undamaged DNA will reanneal with near 100% efficiency if it has accidentally been unwound after unspecific binding of XPC and TFIIH (Fig. 8 A).

XPA and possibly TFIIH can also discriminate between lesions and undamaged DNA (Villani and Tanguy Le Gac, 2000; Dip et al., 2004; Camenisch et al., 2006; Giglia-Mari et al., 2006). These factors may contribute significantly to kinetic proofreading. We estimated the specificity of the NER system by assuming a 100-fold selectivity of XPC, TFIIH, and XPA for damaged over nondamaged DNA. This results in an error fraction of $f < 10^{-8}$ (erroneous incisions per correctly excised damage), which compares with the error rate in DNA

Figure 8. **Specificity of NER.** (A) Damage recognition, DNA unwinding, and kinetic proofreading by XPC, TFIIH, and XPA. We estimated that in ∼40% of the unwinding events after the recognition of a true lesion, the DNA will reanneal, and the repair process must start again. After unspecific binding, this number increases to almost 100%. For simplicity, only binding of XPC, TFIIH, and XPA to the DNA lesion is shown, using the same symbols as in Fig. 4 B. (B) Error fractions in the model for different

dissociation rates of XPC. The affinity ratio for damaged versus undamaged DNA is always 100. The error fraction was calculated as the ratio of mean times to dual excision for a true lesion (τ_L) and an incidental incision on undamaged DNA (τ_U): $f = \tau_L / \tau_U$ High specificity would result in large τ_L (incidental incisions are extremely rare) and thus small f. (C) Mean time to incision for different dissociation rates of XPC.

replication ($\sim 10^{-9}$; Kunkel and Bebenek, 2000). Importantly, when suppressing DNA reannealing in the model (by setting $\varepsilon_{1,2} = 0$), we observed a large increase in the error fraction to $f > 10^{-4}$. Thus, kinetic proofreading enhances molecular discrimination between damaged and nondamaged sites by several orders of magnitude. These results outline a potential proofreading mechanism that utilizes reversible DNA unwinding for achieving the exquisite discriminative power of the NER system.

The model shows that rapidly exchanging proteins are a prerequisite for high specificity. Stably bound proteins would prevent proofreading by stabilizing the unwound DNA repair intermediate; for example, if the XPC dwell time increased 100-fold, the error fraction would increase by six orders of magnitude to $f \sim 10^2$ (Fig. 8 B). However, the rate of NER will be compromised if XPC binds too weakly (Fig. 8 C). Thus, specificity and efficiency of the NER system cannot be maximized simultaneously, and the kinetic design of the NER system must realize a trade-off between these two objectives. The model predicts that a comparatively low XPC affinity, with readily reversible binding of XPC and other repair proteins, results in high specificity and efficiency.

Discussion

We have used a combination of live cell imaging and kinetic modeling to study the formation of DNA repair complexes on the chromatin fiber. Based on extensive kinetic measurements of the binding and dissociation of individual components of the NER machinery, we have computationally reconstructed the assembly dynamics of the multiprotein complexes that catalyze the successive steps of repair. Our results show that the recognition of DNA lesions is strongly rate limiting for repair, whereas after the subsequent DNA unwinding, NER proteins assemble rapidly, randomly, and reversibly into multiprotein complexes. This model reconciles the slow net accumulation kinetics of NER factors at repair sites with their continuous rapid exchange between bound and unbound states (Figs. 2–4). The model makes testable predictions on the rate and capacity of the repair process that have been verified experimentally (Figs. 6 and 7). Moreover, our analysis suggests a kinetic proofreading mechanism for achieving high specificity in lesion recognition that utilizes reversible DNA unwinding and rapidly reversible protein binding (Fig. 8). The model has implications for the kinetic organization of other chromatin-associated processes, including transcription regulation and DNA replication.

Comparison with previous models of protein complex formation on DNA

Our approach differs from previous experimentally based mathematical models that described the kinetic behavior of individual proteins binding to chromatin based on FRAP data (Dundr et al., 2002; Darzacq and Singer, 2008; Gorski et al., 2008; Karpova et al., 2008). In this study, we quantified the formation of multiprotein complexes that are the active units of the DNA repair process. To this end, we developed an integrated kinetic model that simultaneously accounts for the kinetic behavior of seven core NER proteins. Fitting the model to the experimental data yields biochemically plausible estimates for the kinetic parameters of the individual molecular interactions in vivo that account for both the long-term accumulation and the rapid exchange of the NER factors (Fig. 6 and Table I). The model provides a versatile and testable framework for understanding the repair process on the systems level of its interacting factors. At present, techniques for measuring on- and off-rate constants as well as affinities directly in vivo are limited (Michelman-Ribeiro et al., 2009), as are techniques for measuring repair intermediates in vivo. The development of such experimental methods would provide additional tools to further scrutinize and refine the model.

Our results show that the NER system becomes saturated at a remarkably high number of DNA lesions, with an estimated half-saturation at 216,000 lesions per nucleus. For comparison, sunlight is thought to induce up to 30,000 DNA lesions per hour in each skin cell. The maximal rate of repair is estimated at 6,000 lesions per minute, which is consistent with direct measurements of the rate of incision (Kaufmann and Wilson, 1990; Ye et al., 1999). Previous estimates of the time taken to incise a single lesion (~ 4 min) were based on the dissociation rates of individual repair factors from damaged DNA in vivo (Houtsmuller et al., 1999; Rademakers et al., 2003; Zotter et al., 2006). These dissociation rates reflect the k_{off} of individual repair proteins but may not provide information about the time it takes to repair DNA lesions. Indeed, our results imply that repair factors can bind to and dissociate from the same lesion multiple times before it is excised, reconciling the rapid exchange of repair factors and their long-term accumulation at damaged sites. Thus, the mean time to remove a lesion is predicted to be much larger than previous estimates suggested, on average ~ 40 min (Table I). Moreover, there is high stochastic variability in excision time between lesions. At the same time, the NER system has the capacity to process a large number of lesions in parallel, such that the mean time to incise a single lesion or several thousands of them is rather similar. The processing capacity appears to be further regulated by the DDB2 complex that seems to stimulate the recognition of 6-4 PPs by XPC when the concentration of DNA lesions is relatively low. This may be brought about by priming UV-damaged chromatin for the binding of XPC. At higher lesion concentrations, however, DDB2 does not further accelerate the repair of 6-4 PPs (Moser et al., 2005; Nishi et al., 2009).

Experimental testing of model predictions

To validate the predicted kinetics of lesion excision, we monitored the time course over which 6-4 PPs are excised and found good agreement between experiment and model (Fig. 6 G). In view of the fact that no experimental information on the kinetics of DNA repair intermediates was used to parameterize the model, this result attests to the predictive capability of the model. Additional experimental tests have provided further validation of the model. First, the linear dependence of XPG accumulation on the amount of DNA lesions confirms the model prediction that NER is far from saturation under our experimental conditions (Fig. 7, B and C). Second, the relatively low accumulation of XPC in repair-deficient mutants matches the model simulations quite precisely and confirms

the prediction of a comparatively low in vivo affinity of XPC for DNA lesions (Fig. 7 E). Thus, the model has correctly predicted both the time scale of repair and the magnitude of accumulation of NER factors under different experimental conditions.

Efficiency and specificity of NER

The low XPC affinity for damaged DNA and fast reversibility of binding are advantageous for both specificity and efficiency of NER (Fig. 8). The model shows that two distinct mechanisms together can render the error fraction in the recognition of lesions compared with nondamaged DNA as low as $<10^{-8}$: (a) the involvement of multiple factors in damage recognition (XPA and possibly TFIIH) and (b) kinetic proofreading (Hopfield, 1974). These mechanisms greatly increase the specificity of the NER system beyond the poor specificity of XPC (for XPC alone $f_{min} \sim 10^{-2}$; Hey et al., 2002; Hoogstraten et al., 2008). Thus, proofreading may strongly reduce "accidental" repair on non-damaged DNA, which is potentially mutagenic. Kinetic proofreading is naturally realized in our model as a result of the reversibility of the DNA-unwinding steps, which require the binding of NER factors to prevent reannealing. If one or several of these factors bind with higher affinity to a lesion than to un-damaged DNA, the specificity is greatly amplified by the proofreading mechanism. Both specificity-enhancing mechanisms are particularly effective when the recognition factors cannot readily be saturated with DNA lesions. Indeed, we have estimated for XPC and XPA rather low affinities for damaged DNA (K_d of 7–8 μM; Table I). A too-low affinity of XPC, however, would strongly slow down repair. Our results suggest that the observed low XPC affinity mediates an appropriate trade off between specificity and efficiency of NER. In addition, the model indicates that the reversibility of protein binding is beneficial because it prevents the trapping of NER proteins in incomplete (and thus unproductive) repair complexes. Specifically, this explains that the repair rate is maximal at an intermediate k_{off} value for XPC (Fig. 8 C).

General implications of the model for chromatin-associated processes

This study provides a systems-level framework for dissecting the assembly and function of multiprotein machineries acting on chromatin. Our results show that repair factors bind reversibly and assemble mainly stochastically to form enzymatically active protein complexes. In particular, the in vivo data presented in this study and previously (Volker et al., 2001; Rademakers et al., 2003) argue against alternative models that propose irreversible and sequential binding of NER factors (Politi et al., 2005) or NER initiation by proteins other than XPC (Kesseler et al., 2007). In contrast to these earlier models, our results explain the sequentiality of the NER process in a natural manner by the stepwise enzymatic modifications of the DNA substrate at which the proteins assemble. Our model also accommodates cooperative protein–protein interactions, as shown for XPC and TFIIH in the initial unwinding of DNA near a DNA lesion (Yokoi et al., 2000; Sugasawa et al., 2009), and for XPA and ERCC1/XPF (Volker et al., 2001; Tsodikov et al., 2007). Thus, the assembly of NER

complexes at chromatin appears to be governed primarily by protein–DNA interactions and, to a lesser extent, by stable protein–protein interactions. Long-term stability of protein complexes is not necessary because enzymatically active complexes need only be stable for a time interval required to carry out their function (such as DNA unwinding, dual incision, etc.). On the contrary, we find that reversibility of protein binding is beneficial for NER by ensuring high specificity of lesion recognition without compromising efficiency. Our analysis demonstrates the enormous potential of kinetic proofreading for specific damage recognition.

Many proteins involved in transcription and DNA replication have enzymatic activities that may affect histones and other proteins determining chromatin accessibility (van Attikum and Gasser, 2009). Therefore, the formation of chromatin-associated machineries may be orchestrated in time primarily by progressive enzymatic modifications of the chromatin substrate, leaving considerable freedom for the binding mode of individual proteins. Like the components of the NER complex, many transcription factors and RNA polymerases exchange rapidly in the transcription initiation complex, which has been considered inefficient (Dundr et al., 2002; Darzacq et al., 2007; Gorski et al., 2008). However, our analysis suggests that such conclusion may need to be reevaluated when the functioning of multiprotein complexes in terms of specificity and efficiency is taken into account. Our results suggest that proofreading based on reversible protein binding and DNA unwinding, as described for NER, may also support specific target site recognition in transcription. The conflict between specificity and efficiency uncovered in this study is likely a general design principle for chromatin-associated machineries.

Materials and methods

DNA constructs
The XPC cDNA (Hoogstraten et al., 2008) was ligated in frame with mVenus and mOrange (Shaner et al., 2004; Kremers et al., 2006), resulting in XPC-mVenus and XPC-mOrange. In addition, XPA cDNA (Rademakers et al., 2003) was ligated in frame with mOrange, yielding mOrange-XPA. Constructs were transiently transfected in several NER mutant cell lines at low levels using Lipofectamine 2000 (Invitrogen) according to the manufacturer's instructions. RPA70 cDNA (Henricksen et al., 1994) was cloned in frame with EGFP in pEGFP-N1 (Takara Bio Inc.) and stably expressed in SV40-transformed MRC5 human fibroblasts. The EGFP–histone H4 plasmid was provided by S. Diekmann (Leibniz Institute for Age Research, Jena, Germany).

Cell lines
Cell lines stably expressing EGFP-tagged NER proteins used in this study were human fibroblasts XPC-deficient XP4PA-SV– expressing XPC-EGFP (Hoogstraten et al., 2008), XPA-deficient XP2OS-SV–expressing EGFP-XPA (Rademakers et al., 2003), XPB-deficient XPCS2BA-SV–expressing XPB-EGFP (Hoogstraten et al., 2002), and wild-type MRC5-SV–expressing RPA70-EGFP. The following CHO cells were used: XPG/ERCC5-deficient UV135–expressing XPG-EGFP (Zotter et al., 2006), ERCC1-deficient 43-3B–expressing ERCC1-GFP (Houtsmuller et al., 1999), wild-type CHO9-expressing EGFP-PCNA (Essers et al., 2005), and CHO K1. The expression level of all EGFP-tagged repair proteins is comparable with the level of endogenous proteins as shown by Western blot analysis (Houtsmuller et al., 1999; Hoogstraten et al., 2002, 2008; Rademakers et al., 2003; Essers et al., 2005; Zotter et al., 2006). The following NER mutant cell lines were used: human XP-B (XPCS2BA-SV; Vermeulen et al., 1994), XP-A (XP12RO-SV; Satokata et al., 1992), XP-F (XP2YO-SV; Yagi et al., 1991), CHO XP-B/ERCC3 (27.1; Hall et al., 2006), XP-G/ERCC5

(UV135; MacInnes et al., 1993), and ERCC1 (43-3B; van Duin et al., 1986). All cell lines expressing EGFP-tagged NER proteins were cultured in a 1:1 mixture of DME/Ham's F10 medium. All media contained glutamine (Invitrogen) supplemented with antibiotics and 10% FCS, and all cells were cultured at 37°C in an atmosphere of 5% CO_2.

Western blotting
Cell extracts of parental MRC5 cells and MRC5 cells expressing RPA70-EGFP were generated by sonication, separated by 8% sodium dodecyl sulfate polyacrylamide gel electrophoresis, and transferred to nitrocellulose membranes. Expression of RPA70-EGFP was analyzed by immunoblotting with mouse monoclonal anti-RPA70 antibodies (B-6/sc-28304; 1:1,000; Santa Cruz Biotechnology, Inc.) and mouse monoclonal anti-EGFP antibodies (1:1,000; Roche) followed by a secondary antibody (donkey anti–mouse 800CW; 1:5,000; LI-COR Biosciences) and detection using an infrared imaging-scanning system (Odyssey; LI-COR Biosciences).

UV irradiation
For all experiments, cells were irradiated with a UV source containing four UV lamps (9-W TUV PL-S; Philips) above the microscope stage. The UV dose rate was measured to be 3 W/m^{-2} at 254 nm. For induction of local UV damage, cells were UV irradiated through a polycarbonate mask (Millipore) with pores of 5 µm and subsequently irradiated for 39 s (100 $J.m^{-2}$; Moné et al., 2004; Luijsterburg et al., 2007).

Microscopic analysis
Binding kinetics were measured on a widefield fluorescence microscope (Axiovert 200M; Carl Zeiss, Inc.) equipped with a 100× Plan Apochromat 1.4 NA oil immersion lens (Carl Zeiss, Inc.) and a xenon arc lamp with monochromator (Cairn Research Ltd.). Images were recorded with a cooled charge-coupled device camera (CoolSNAP HQ; Roper Industries) using MetaMorph imaging software (version 6.1; MDS Analytical Technologies). FLIP, inverse FRAP, and photoconversion experiments were performed on a confocal microscope (LSM 510 META; Carl Zeiss, Inc.) equipped with a 63× Plan A 1.4 NA oil immersion lens (Carl Zeiss, Inc.), a 60-mW argon laser (488 and 514 nm), a 5-mW helium neon 1 (543 nm) laser, a 15-mW helium neon 2 (633 nm) laser, two photomultiplier tubes, and a META detector. Images were recorded using imaging software (LSM; Carl Zeiss, Inc.). Both microscopes were equipped with an objective heater and a climate chamber. Cells were examined in microscopy medium (137 mM NaCl, 5.4 mM KCl, 1.8 mM $CaCl_2$, 0.8 mM $MgSO_4$, 20 mM D-glucose, and 20 mM Hepes) at 37°C.

Binding kinetics
Cells were grown in glass-bottom dishes (MatTek) and locally UV irradiated as described previously (Moné et al., 2004; Luijsterburg et al., 2007). Individual cells were subsequently monitored for up to 6 h. Accumulation of EGFP-tagged repair proteins after local irradiation was quantified with Objective Image software. Time courses were normalized with respect to the plateau level. Start of the UV irradiation was defined as t = 0. The bound fraction of EGFP-tagged NER proteins in the local damage was calculated by the following equation: bound percent = $(I_{spot} - I_{outspot})$ × $pixels_{spot}/(I_{nucleus} - I_{background})$ × $pixels_{nucleus}$; where I_{spot} and $I_{outspot}$ are the mean pixel intensities inside the damaged spot and outside the spot, respectively. $I_{nucleus}$ is the mean pixel intensity of the nucleus, including the spot, and $I_{background}$ is the mean pixel intensity outside of the cell.

FLIP
FLIP analysis was performed by continuously bleaching a third of a locally UV-irradiated nucleus opposite to the site of damage at 100% laser intensity (488-nm argon ion laser) as previously described (Hoogstraten et al., 2002; Luijsterburg et al., 2007). A 60-mW argon ion laser was used for excitation at 488 nm, passed onto the sample by a 490-nm dichroic mirror, and emission light was filtered by a 505–550-nm emission filter. Fluorescence in the locally damaged area was monitored with low laser intensity. All values were background corrected. We chose experimental conditions (extended bleaching area and high bleaching frequency) in which an EGFP-tagged repair protein that dissociates from sites of DNA damage will likely be bleached before rebinding to sites of damage. For example, a protein with a fast on rate of 10^5 $M^{-1}s^{-1}$ would take of the order of 30 s to rebind to DNA damage occurring at a concentration of 0.35 µM (as in the experiments reported in this study). By comparison, diffusion over the typical nuclear dimension of 5 µm to hit the bleaching area with a comparatively low diffusion coefficient of 10 $µm^2$ s^{-1} (as measured for TFIIH; Hoogstraten et al., 2002; Luijsterburg et al., 2007) would require on average only 1.25 s.

FLIP experiments with pertubation of NER
To stall NER at the repair synthesis stage, we added inhibitors of repair synthesis and DNA ligation, i.e., HU at 100 mM and AraC at 10 µM (Smith and Okumoto, 1984; Mullenders et al., 1987) ∼1 h before local UV-C irradiation. Subsequently, the cells were locally irradiated, and we determined the dissociation kinetics of NER factors by FLIP when the maximal amount of bound proteins was reached.

Photoconversion experiments
XP4PA cells transiently expressing low levels of XPC-mOrange were locally irradiated with UV-C light. Cells were monitored in multitrack mode. A 5-mW helium neon laser was used for excitation at 543 nm, passed onto the sample by a 543-nm dichroic mirror, and emission light was filtered by a 560–615-nm emission filter. Simultaneously, a 15-mW helium neon laser was used for excitation at 633 nm, passed onto the sample by a 633-nm dichroic mirror, and emission light was filtered by a 650-nm long-pass emission filter. Images of 512 × 512 pixels were acquired with a scan time of 1.97 s (two means per line) at zoom 5 in the 543 and 633 channels. After three images, a region of 90 × 90 pixels containing the damaged area was photoconverted (15 iterations) with maximal 488-nm laser intensity (AOTF 100%; Kremers et al., 2009). Fluorescence in the locally damaged area was monitored with low laser intensity for at least 25 images with a 5-s time interval between images in the 543 and 633 channels. The loss of fluorescence at the locally damaged in the 633 channel (FLIP; caused by dissociation of photoconverted molecules) and the recovery of fluorescence in the 543 channel (FRAP; caused by association of nonphotoconverted molecules) were quantified. Curves represent the FLIP from which the FRAP has been subtracted, which is a measure for the dissociation kinetics.

Inverse FRAP
XP4PA cells transiently expressing low levels of XPC-mOrange were locally irradiated with UV-C light. After three images, the entire nucleus except for the locally damaged area was bleached (15 iterations) with maximal 488-nm laser intensity (AOTF 100%). The reequilibration of bleached and nonbleached molecules was monitored with low laser intensity for at least 25 images with an 8-s time interval between images in the 543 channel. The loss of fluorescence at the locally damaged was quantified (ImageJ; National Institutes of Health), which is a measure for the dissociation kinetics.

Immunofluorescent labeling of 6-4 PP and CPD
XP4PA cells expressing XPC-EGFP were seeded on poly-D-lysine–coated coverslips, irradiated through 5-µm pores at 100 $J.m^{-2}$, and fixed at different time points after UV irradiation (directly after UV and 1, 2, 4, and 8 h after UV). Control cells were mock treated (i.e., not irradiated) and fixed. Cells were fixed with 4% formaldehyde in PBS for 15 min at 4°C, permeabilized in 0.5% Triton X-100 (Serva) in PBS for 5 min, and incubated with 100 mM glycine in PBS for 10 min to block unreacted aldehyde groups. Subsequently, DNA was denatured with 0.1 M HCl for 10 min at 37°C, and cells were blocked in 10% BSA in PB for 15 min. Cells were rinsed with PB (130 mM KCl, 10 mM Na_2HPO_4, and 2.5 mM $MgCl_2$, pH 7.4) and equilibrated in WB (PB containing 0.5% BSA, 0.2% gelatin, and 0.05% Tween 20; Sigma-Aldrich). Antibody steps and washes were performed in WB. The primary antibodies mouse anti-CPD (1:400; Nordic Biosite) and mouse anti–6-4 PP (1:500; Nordic Biosite) were incubated overnight. Detection was performed using donkey anti–mouse Ig coupled to Alexa Fluor 546 (1:1,000; Jackson ImmunoResearch Laboratories, Inc.). Samples were mounted in Mowiol, and images were acquired on a confocal microscope (LSM 510; see Microscopic analysis). The fluoresence intensity of at least 50 local UV spots was measured using ImageJ software. The measured intensities were background corrected (using nonirradiated control images) and normalized to 1 (using cells that were fixed immediately after local UV irradiation; i.e., 0-h time point).

Estimation of the amount of locally inflicted lesions
To estimate the concentration of 6-4 PPs inflicted using local UV-C irradiation at 100 $J.m^{-2}$ through 5-mm pores of a polycarbonate mask, we used available measurements of the absolute amounts of 6-4 PPs and CPDs inflicted upon UV-C irradiation of CHO cells (Perdiz et al., 2000). These data demonstrate that the number of inflicted 6-4 PPs and CPDs does not increase linearly with increasing UV dose. By extrapolating the data of Perdiz et al. (2000), we estimate that global UV-C irradiation at 100 $J.m^{-2}$ produces ∼6 ×10^5 6-4 PPs genome wide (Fig. S1 A). However, by irradiating cells locally through 5-µm pores, we irradiate ∼10% of the nuclear volume and thus produce ∼6 × 10^4 6-4 PPs in the locally damaged area,

which translates to a nuclear concentration of 0.3 µM (assuming a nuclear volume of 0.3 pL). For comparison, global UV-C irradiation at 16 J.m^{-2}, a dose often used to saturate NER, produces 3×10^5 6-4 PPs genome wide. In agreement with the nonlinear increase of 6-4 PPs at increasing UV-C fluencies, we show that the amount of immobilized XPG-EGFP does not increase beyond ~10% of the protein pool when the UV-C dose is increased beyond 100 J.m^{-2} (Fig. S1 B). However, when we increase the amount of inflicted 6-4 PPs by irradiating a larger nuclear area (by using pores with 3, 5, and 8 µm, respectively), we obtain a linear increase in the amount of immobilized XPG-EGFP up to 22% of the protein pool (Fig. 7 C). These results show that (a) the used UV-C dose is not a quantitative measure for the amount of inflicted DNA lesions and (b) the lesion concentration upon local irradiation at 100 J.m^{-2} (5-µm pores) is only about twofold higher than the concentration after global irradiation at 16 J.m^{-2}, whereas the absolute amount of damages is about fivefold lower (~60,000 6-4 PPs). Thus, we estimated that our standard local UV-C irradiation introduces ~60,000 6-4 PPs, corresponding to a nuclear concentration of 0.3 µM.

Mathematical model

The model structure translates into 214 nonlinear differential equations for the various protein complexes that can be formed at the DNA repair intermediates and the free concentrations of the repair proteins. Nucleoplasmic diffusion of NER factors is not considered explicitly, as it is much faster than the characteristic times for binding and release at damage sites (Houtsmuller et al., 1999; Rademakers et al., 2003; Zotter et al., 2006).

The concentration of any possible state (repair intermediate with bound proteins) is indicated by y_π^R. The superscript index, R, refers to the repair intermediate that is defined by the modification of the DNA substrate (damaged DNA I, partially unwound DNA II, fully unwound DNA III, incised DNA IV, resynthesized DNA V, and chromatinized DNA VI). The presence of the individual proteins is encoded in a binary way in the tuple, π. The tuple π consists of seven elements: one for each protein $p \in \{C, T, G, A, F, R, \text{and } P\}$. Each protein variable $\pi(p) \in \{1, 0\}$ reveals if the protein is bound, $\pi(p) = 1$, or not, $\pi(p) = 0$. If the protein cannot bind to the given repair intermediate R, $\pi(p) = 0$ by definition.

In principle, each repair intermediate can have 2^N possible states, depending on which proteins are bound, where N is the number of proteins that can bind to the given DNA substrate. However, in two cases, we restrict the number of states as follows. First, to damaged DNA (repair intermediate I), XPC must bind first before TFIIH can bind so that the tuple with $C = 0$, $T = 1$ is excluded, and consequently, $2^{2-1} = 3$ states exist for repair intermediate I. Second, XPF/ERCC1 (F) can only bind if XPA (A) is already bound (Table S1), so that any tuple with $A = 0$ and $F = 1$ is excluded. In repair intermediates II and III, where six proteins can bind, this results in $2^6 - 2^4 = 48$ possible states. For repair intermediate IV, we have $2^7 - 2^5 = 96$ possible states. Repair intermediate V has $2^3 = 8$ states, and repair intermediate VI has 4 states for the binding of PCNA and RPA only. The time evolution of the 207 states of repair intermediates is governed by following system of differential equation:

$$\frac{d}{dt}y_\pi^R = \sum_{p \text{ in } R} \underbrace{(-1)^{\pi(p)} l_p^R y_\pi^R \big|_{\pi(p)=1}}_{\text{protein dissociation}} + \underbrace{(-1)^{1+\pi(p)} k_p^R C_p(t) y_\pi^R \big|_{\pi(p)=0}}_{\text{protein binding}} + \underbrace{E\left(y_\pi^R\right)}_{\text{enzymatic reactions}}, \quad (1)$$

where for each $R = \text{I},\dots,\text{VI}$ all allowed tuples π are to be considered.

The on-rate constant of protein p for a certain repair intermediate R is given by k_p^R and the corresponding off-rate constant by l_p^R. The time-dependent concentrations of free protein C_p are determined by Eq. 2.

The enzymatic reactions are denoted by $E(y_\pi^R)$ if a state has no in- or outgoing enzymatic reaction, $E = 0$. For damaged DNA ($R = \text{I}$), we have

$$E\left(y_{00}^{\text{I}}\right) = \varepsilon_1 y_{000000}^{\text{II}} + \varepsilon_2 y_{000000}^{\text{III}} \quad \text{and} \quad E\left(y_{11}^{\text{I}}\right) = -\alpha y_{11}^{\text{I}}.$$

For partially unwound DNA ($R = \text{II}$),

$$E\left(y_{000000}^{\text{II}}\right) = -\varepsilon_1 y_{000000}^{\text{II}}, \quad E\left(y_{110000}^{\text{II}}\right) = \alpha y_{11}^{\text{I}},$$

$$E\left(y_{111101}^{\text{II}}\right) = -\alpha' y_{111101}^{\text{II}}, \quad \text{and} \quad E\left(y_{111111}^{\text{II}}\right) = \alpha' y_{111111}^{\text{II}}.$$

For fully unwound DNA ($R = \text{III}$),

$$E\left(y_{000000}^{\text{III}}\right) = -\varepsilon_2 y_{000000}^{\text{II}}, \quad E\left(y_{011111}^{\text{III}}\right) = -\beta y_{011111}^{\text{III}},$$

$$E\left(y_{111101}^{\text{III}}\right) = \alpha' y_{111101}^{\text{II}}, \quad \text{and} \quad E\left(y_{111111}^{\text{III}}\right) = -\beta y_{111111}^{\text{III}} + \alpha' y_{111111}^{\text{II}}.$$

For incised ($R = \text{IV}$) and resynthesized DNA ($R = \text{V}$),

$$E\left(y_{111111}^{\text{IV}}\right) = \beta y_{111111}^{\text{III}} \quad \text{and} \quad E\left(y_{011}^{\text{V}}\right) = \gamma y_{0001011}^{\text{IV}} - \delta y_{011}^{\text{V}}.$$

Finally, for rechromatinized DNA ($R = \text{VI}$),

$$E\left(y_{011}^{\text{VI}}\right) = \delta y_{011}^{\text{V}}.$$

The time evolution of the free concentrations of the C_p of the proteins $p \in \{C, T, G, A, F, R, \text{and } P\}$ is governed by the following seven differential equations:

$$\frac{d}{dt}C_p = \sum_{R=\text{I}}^{\text{VI}} \sum_\pi \delta_{p1} l_p^R y_\pi^R - \delta_{p0} k_p^R C_p y_\pi^R. \quad (2)$$

The second sum runs over all allowed index tuples π for the given repair intermediate R. The Kronecker δ,

$$\delta_{ij} = \begin{cases} = 1 & \text{if} \quad i = j \\ = 0 & \text{if} \quad i \neq j \end{cases},$$

ensures that proteins only bind to complexes not containing the protein yet and only leave complexes containing them.

The accumulation curves of the core proteins XPC, TFIIH, XPG, XPA, ERCC1/XPF, RPA, and PCNA are generated by summing over the concentration of all states that contain the respective protein. The initial conditions of Eqs. 1 and 2 for simulating protein accumulation after UV damage are given by the free concentrations of all proteins equal to the total concentrations and the value for the initial damage concentration of y_{00}^{I} (0.33 µM); all other states empty. For simulating the FLIP curves of a given protein, its on-rate constants are set to zero (corresponding to the simplifying assumption that any unbound fluorescent molecule is bleached before it rebinds). The initial conditions are given by the state of the system during the response to UV damage at the time point at which the FLIP experiment was started (i.e., 600s for XPC and ERCC1/XPF, 900s for XPG and TFIIH, 2,000s for XPA, and 7,200s for PCNA).

Fit of the model to the data

The FLIP measurements indicate that most repair proteins bind to the DNA lesions without noticeable binding cooperativity with other proteins (except for strictly sequential binding of XPC and TFIIH and strong cooperativity between ERCC1/XPF and XPA). Rather, a sequence of binding events appears to be established by the enzymatic action of protein complexes on the chromatin (e.g., through unwinding of the DNA and excision of the lesion, etc.) that changes the affinity of the repair proteins for the chromatin substrate. Random protein binding may create a large number of protein complex species (most of them being partially assembled complexes), and the question arises as to which kind of measurements need to be conducted to quantify their assembly dynamics.

As a simple case, consider the formation of a multiprotein complex from N reversibly binding components on a single repair intermediate of constant (or slowly varying) concentration, B. If the proteins bind independently of one another and their free concentrations are sufficiently large, the kinetic equations for the concentrations of the various complexes y_π (compare with Eq. 1) can be integrated to yield

$$y_\pi = B \underbrace{\prod_i \frac{k_i'}{k_i' + l_i}\left(1 - \exp\left\{-(k_i' + l_i)t\right\}\right)}_{\text{proteins } i \text{ present}} \underbrace{\prod_j \frac{k_j' \exp\left\{-(k_j' + l_j')t\right\} + l_j}{k_j' + l_j}}_{\text{proteins } j \text{ absent}},$$

where the indices i and j stand for the protein species that must bind and dissociate, respectively, to form the complex; i.e., $\pi(i) = 1$ and $\pi(j) = 0$.

As unbound proteins are in excess, we have assumed their concentrations as constant and defined the first-order binding rate constants $k_i' = k_i C_i$.

The term

$$B \frac{k_i'}{k_i' + l_i} \left(1 - \exp\left\{ -(k_i' + l_i')t \right\} \right)$$

is the net accumulation curve of protein i (and the terms with index j are the corresponding complements). Therefore, the composition of any protein complex formed from independently binding proteins can be inferred when the accumulation curves of all individual proteins are known.

From experimentally measured accumulation curves, we can determine the amplitude,

$$A_i = B \frac{k_i'}{k_i' + l_i}, \qquad (3)$$

and the characteristic time of accumulation,

$$t_{\mathrm{acc},i} = \frac{1}{k_i' + l_i'}, \qquad (4)$$

allowing us to separately identify the on- and off-rate constants k_i' and l_i, provided that the total amount of binding sites B (i.e., the number of DNA lesions) is known. FLIP measurements provide an estimate of the characteristic dwell times of the repair protein in the complexes

$$t_{\mathrm{dwell},i} = \frac{1}{l_i'}. \qquad (5)$$

Having joint measurements of A_i and $t_{\mathrm{acc},i}$ (from the accumulation curves) and $t_{\mathrm{dwell},i}$ (from the FLIP experiments), we can estimate all three parameters on the right-hand sides of Eqs. 3–5: k_i', l_i, and B; note that an independent estimate of B is no longer needed (but nevertheless exists in our data and proves useful for the fit of the full model). Thus, the simplified model of protein complexes assembling on a single kind of DNA repair intermediate is completely identifiable with two types of measurement: (1) accumulation kinetics of all individual proteins (in absolute concentration scale) and (2) dwell times of all proteins.

We have checked numerically on surrogate data that this property also holds when a particular protein complex has enzymatic activity that decreases the concentration of the binding substrate (to be specific, we chose the multiprotein complex in which all components are bound). B becomes a function of time, $B = B_0 f(t; k_i', l_i, \alpha)$. The additional parameter, the enzymatic rate constant α, can also be estimated from the given data as long as it is not much faster than k_i'. If α is much faster than the k_i', the reaction is limited by protein binding. Then, α has negligible control on the kinetics so that its actual value is of little interest.

In the full model, we have several DNA repair intermediates, and protein complexes of appropriate composition have enzymatic activities that convert one repair intermediate into another. This model has no explicit solution; therefore, its identifiably can not be determined analytically. However, guided by the aforementioned considerations, we have found that the following experimental data yielded reliable estimates of the model parameters: accumulation kinetics of all proteins in the model, dwell times of all proteins for unperturbed NER, total amounts of repair proteins in the nucleus and inflicted lesions together with dwell of XPC, XPA, PCNA, and ERCC1/XPF in various settings of stalled NER, and a few appropriate restrictions on the parameter space.

In particular, the FLIP experiments for NER stalled at various repair intermediates help to discriminate the dwell times of the proteins at different repair intermediates. To constrain the model, we included several experimental observations and simplifications as follows.

Because RPA binds to long stretches of single-stranded DNA more strongly than to short stretches, we constrained the RPA affinity to fully unwound DNA (repair intermediate III) to be at least five times as large as to partially unwound DNA (repair intermediate II; Blackwell and Borowiec, 1994). However, RPA should have the same affinity for fully unwound DNA (repair intermediate III) and incised DNA (repair intermediate IV) because the single-stranded–binding partner stays the same. All proteins except RPA (i.e., XPC, TFIIH, XPG, XPA, and ERCC1/XPF) have the same affinity for partially unwound (repair intermediate II) and fully unwound DNA (repair intermediate III). For XPC, this is implied by the FLIP data, which show that the XPC dissociation rate changes only after formation of the full

Table II. **Values of the enzymatic rate constants**

Enzymatic rate	k_{cat}
	s^{-1}
Partial unwinding α	0.08 (0.06; 0.11)
Full unwinding α'	0.74 (0.59; 0.74)
Incision β	4.1 (3.8; 6.0)
Resynthesis γ	0.05 (0.04; 0.06)
Rechromatinization δ	0.012 (0.012; 0.013)
Reannealing ε_1	3.1 (2.5; 24.1)
Reannealing ε_2	11.0 (4.9; 11.1)

Reference parameter set and 90% confidence intervals (in parentheses) are shown.

preincision complex (and likely after dual incision). For the other proteins, we make the same assumption because their binding does not appear to require large-scale DNA unwinding. These assumptions reduce the number of distinct binding and dissociation rate constants. The binding of TFIIH is dependent on the binding of the damage recognition factor XPC to the DNA lesion (i.e., repair intermediate I), and the dimer XPF/ERCC1 can only bind if XPA is present (Volker et al., 2001).

To systematically explore the parameter space of the model, we used an MCMC method (Press et al., 2007) for minimizing the residual sum of squares (χ^2) between the data shown in Fig. 5 (A–D) and the corresponding model simulations. This procedure yielded a distribution of the best-fit values for each parameter. Tables I and II show the best-fit values (smallest χ^2) and 90% confidence intervals (given by the parameter distributions) for the 47 parameters, 20 pairs of k_{on} (k) and k_{off} (l) values, five catalytic rate constants, k_{cat} (α, α', β, γ, and δ), and two reannealing rate constants (ε_1 and ε_2). The confidence intervals are comparably small for all parameters except for the reannealing rate constants ε_1 and ε_2. However, the reannealing of a $\sim$30-nucleotide stretch of DNA is very fast, and we found that the precise values do not matter as long as the characteristic times for the reannealing are in the subsecond range (as shown in Table II). In this case, the reannealing of the DNA is limited by the dissociation rates of the proteins stabilizing the unwound state, as one can reasonably expect. In addition, the dissociation constants $K_D = k_{off}/k_{on}$ were calculated; characteristic times for enzymatic reactions are given by $1/k_{cat}$. The mean times to produce repair intermediates τ are also listed (see following paragraph).

Characteristic times

The characteristic time τ (y^R_π) of the state $y^R(t)$ is defined by the first moment of the distribution divided by the zeroth moment. With the mth moment defined by

$$\mu^{(m)} = \int t^m \, y^R_\pi(t)\, dt,$$

where the characteristic time is

$$\tau = \frac{\mu^{(1)}}{\mu^{(0)}},$$

and the standard deviation is

$$\sigma = \sqrt{\frac{\mu^{(2)}}{\mu^{(0)}} - \tau^2}. \qquad (6)$$

The characteristic times to partial unwinding (τ_{part}; i.e., $R = \mathrm{I}$), to full unwinding (τ_{full}; i.e., $R = \mathrm{II}$), and to incision (τ_{inc}; i.e., $R = \mathrm{III}$) are given by

$$\tau_R = \frac{\int_0^\infty t \sum_{x=\mathrm{I}}^R \sum_\pi y^x_\pi(t)\, dt}{\int_0^\infty \sum_{x=\mathrm{I}}^R \sum_\pi y^x_\pi(t)\, dt}.$$

The first sum runs over all repair intermediates proceeding and the repair intermediate itself. The second sum runs over all tuple π and is thereby

summing over the concentrations of all states within a given repair intermediate. To ensure convergence of the integrals, the time to resynthesis is calculated by tracking all repair intermediates before resynthesis using the equation

$$\tau_{\text{syn}} = \frac{\int_0^\infty t\left(y_{00}^{\text{I}}(0) - \left(\sum_\pi y_\pi^{\text{IV}}(t) + \sum_\pi y_\pi^{\text{I}}(t)\right)\right)dt}{\int_0^\infty y_{00}^{\text{I}}(0) - \left(\sum_\pi y_\pi^{\text{IV}}(t) + \sum_\pi y_\pi^{\text{I}}(t)\right)dt}.$$

The time to chromatinize is calculated analogously:

$$\tau_{\text{chrom}} = \frac{\int_0^\infty t\left(y_{00}^{\text{I}}(0) - \sum_\pi y_\pi^{\text{V}}(t)\right)dt}{\int_0^\infty \left(y_{00}^{\text{I}}(0) - \sum_\pi y_\pi^{\text{V}}(t)\right)dt}. \tag{7}$$

The corresponding standard deviations are calculated in the same manner, according to Eq. 6. With the reference parameter set, these definitions yield for partially unwound DNA ($\tau_{\text{part}} = 35 \pm 30$ min), fully unwound DNA ($\tau_{\text{full}} = 41 \pm 36$ min), incised DNA ($\tau_{\text{inc}} = 41 \pm 36$ min), resynthesized DNA ($\tau_{\text{syn}} = 2.0 \pm 0.7$ h), and rechromatinized DNA ($\tau_{\text{chrom}} = 2.2 \pm 0.7$ h). The high standard deviations indicate that there are considerable stochastic variations in timing from lesion to lesion.

Michaelis–Menten approximation

As a phenomenological approximation for the dependence of the incision rate v on the amount of initial damage D, consider the Michaelis–Menten equation

$$v(t) = v_{\text{max}} \frac{D(t)}{K_{\text{M}} + D(t)}.$$

We approximate the time-dependent change of the total damage by

$$\frac{dD}{dt} = -v(t),$$

and separation of variables by

$$v_{\text{max}}\, dt = -\frac{K_{\text{m}} + D(t)}{D(t)}\, dD,$$

To obtain the characteristic time for repair,

$$\tau = \frac{1}{D(0)}\int_0^\infty D(t)\, dt = \frac{1}{2}\frac{D(0)}{v_{\text{max}}} + \frac{K_{\text{M}}}{v_{\text{max}}}.$$

Eq. 7 predicts that the time to incision will rise as a linear function of initial damage $D(0)$ (compare with Fig. S4 B). Therefore, we approximated the initial part of the τ_{inc} curve in Fig. S4 B for the characteristic time to incision versus the initial amount of damage by a straight line, yielding a slope of approximately

$$\frac{1}{2}\frac{1}{v_{\text{max}}} = \frac{5\,\text{min}}{60,000\,\text{lesions}},$$

and consequently, the maximal rate of repair (of 6-4 PPs) per cell nucleus is $v_{\text{max}} = 6,000$ lesions/min. The interpolated intersection with the ordinate is approximately at $K_{\text{M}}/v_{\text{max}} = 36$ min, yielding a half-saturation constant of $K_{\text{M}} = 216,000$ lesions. Thus, there is very considerable capability for the parallel processing of DNA lesions by the NER system.

Specificity of NER

In this study, we assess the specificity of NER when it would be determined by the binding of XPC only. We assume that binding of XPC may trigger DNA unwinding and the assembly of the NER complex regardless of whether it binds to DNA lesions. Measurements indicate that a DNA-bound XPC molecule occupies 20–30 base pairs of DNA (Sugasawa et al., 1998; Min and Pavletich, 2007). Given that a diploid human cell has $6.4\ 10^9$ base pairs, we estimate approximately between 2 and 3×10^8 unspecific binding sites (B) for XPC and thus the NER complex. This translates to a nuclear concentration of 1.21–1.77 mM (assuming a nuclear volume of 0.3 pL). The affinity of XPC for unspecific binding is

100-fold lower than for DNA lesions (Hey et al., 2002; Hoogstraten et al., 2008), which is 0.78 mM for our model parameters. On average, the concentration of XPC bound to undamaged sites will be

$$[\text{XPC} - \text{B}] = \frac{[\text{XPC}]_{\text{free}}[\text{B}]_{\text{free}}}{K_D}, \quad \text{where}$$

$$[\text{XPC} - \text{B}]_{\text{total}} = [\text{XPC}]_{\text{free}} + [\text{XPC-B}] \quad \text{and}$$

$$[\text{B}]_{\text{total}} = [\text{B}]_{\text{free}} + [\text{XPC-B}].$$

The solution indicates that between 61 and 69% of the XPC molecules (15,000–18,000 molecules) are nonspecifically bound at any given time. This number agrees with recent measurements on XPC-GFP in vivo, where 50% of the XPC pool was shown to be transiently bound to chromatin at all times (Hoogstraten et al., 2008). From our model, we estimate that it takes between 6 and 10 min to incision if XPC is already bound; consequently, there should be $\approx 10^4$–10^5 incisions/h at undamaged sites of the genome if no further mechanisms were in place to prevent such erroneous incisions. However, our model naturally accounts for a kinetic proofreading mechanism that, under certain conditions, can strongly enhance the specificity of NER. In kinetic proofreading, an enzyme–substrate complex is taken through a series of high energy intermediates at the expense of metabolic energy before the final committing reaction step can take place. In the passage through these intermediate states, the stability of the complex is tested several times, thus leading to a more faithful discrimination between the true substrate and close analogues than could be achieved by a single binding step (Hopfield, 1974). In our model, kinetic proofreading naturally occurs through reversible unwinding of the DNA around a lesion. As the DNA will reanneal spontaneously when the stabilizing preincision proteins (stochastically) dissociate, the binding of these proteins is subjected to a stringent stability test.

The affinities of XPC and XPA for DNA depend on the distorted helical structure and the presence of the lesion, respectively (Camenisch et al., 2006; Maillard et al., 2007). Moreover, the subunit composition of TFIIH is different when binding to a DNA lesion as compared with its engagement in transcription (Giglia-Mari et al., 2006) so that it may also bind with different affinities to damaged and nondamaged DNA (Villani and Tanguy Le Gac, 2000; Dip et al., 2004). Additionally, XPA preferentially binds to kinks in the helical DNA structure that are induced by DNA lesions and therefore can also contribute to the discrimination between damaged and nondamaged DNA (Camenisch et al., 2006).

The affinities of XPC and XPA for DNA depend on the distorted helical structure and the presence of the lesion, respectively (Camenisch et al., 2006; Maillard et al., 2007). Moreover, the subunit composition of TFIIH is different when binding to a DNA lesion as compared with its engagement in transcription (Giglia-Mari et al., 2006) so that it may also bind with different affinities to damaged and nondamaged DNA (Villani and Tanguy Le Gac, 2000; Dip et al., 2004). Additionally, XPA preferentially binds to kinks in the helical DNA structure that are induced by DNA lesions and therefore can also contribute to the discrimination between damaged and nondamaged DNA (Camenisch et al., 2006).

Online supplemental material

Fig. S1 shows locally inflicted lesions. Fig. S2 shows immunoblot analysis of RPA70-EGFP cells. Fig. S3 shows that cells analyzed by FLIP remain repair competent. Fig. S4 shows the rate of NER. Table S1 shows model assumptions. Online supplemental material is available at http://www.jcb.org/cgi/content/full/jcb.200909175/DC1.

References

Aboussekhra, A., M. Biggerstaff, M.K. Shivji, J.A. Vilpo, V. Moncollin, V.N. Podust, M. Protić, U. Hübscher, J.M. Egly, and R.D. Wood. 1995. Mammalian DNA nucleotide excision repair reconstituted with purified protein components. *Cell.* 80:859–868. doi:10.1016/0092-8674(95)90289-9

Araújo, S.J., E.A. Nigg, and R.D. Wood. 2001. Strong functional interactions of TFIIH with XPC and XPG in human DNA nucleotide excision repair, without a preassembled repairosome. *Mol. Cell. Biol.* 21:2281–2291. doi:10.1128/MCB.21.7.2281-2291.2001

Black, J.C., J.E. Choi, S.R. Lombardo, and M. Carey. 2006. A mechanism for coordinating chromatin modification and preinitiation complex assembly. *Mol. Cell.* 23:809–818. doi:10.1016/j.molcel.2006.07.018

Blackwell, L.J., and J.A. Borowiec. 1994. Human replication protein A binds single-stranded DNA in two distinct complexes. *Mol. Cell. Biol.* 14:3993–4001.

Camenisch, U., R. Dip, S.B. Schumacher, B. Schuler, and H. Naegeli. 2006. Recognition of helical kinks by *xeroderma pigmentosum* group A protein triggers DNA excision repair. *Nat. Struct. Mol. Biol.* 13:278–284. doi:10.1038/nsmb1061

Camenisch, U., R. Dip, M. Vitanescu, and H. Naegeli. 2007. *Xeroderma pigmentosum* complementation group A protein is driven to nucleotide excision repair sites by the electrostatic potential of distorted DNA. *DNA Repair (Amst.).* 6:1819–1828. doi:10.1016/j.dnarep.2007.07.011

Coin, F., V. Oksenych, and J.M. Egly. 2007. Distinct roles for the XPB/p52 and XPD/p44 subcomplexes of TFIIH in damaged DNA opening during nucleotide excision repair. *Mol. Cell.* 26:245–256. doi:10.1016/j.molcel.2007.03.009

Darzacq, X., and R.H. Singer. 2008. The dynamic range of transcription. *Mol. Cell.* 30:545–546. doi:10.1016/j.molcel.2008.05.009

Darzacq, X., Y. Shav-Tal, V. de Turris, Y. Brody, S.M. Shenoy, R.D. Phair, and R.H. Singer. 2007. In vivo dynamics of RNA polymerase II transcription. *Nat. Struct. Mol. Biol.* 14:796–806. doi:10.1038/nsmb1280

de Laat, W.L., E. Appeldoorn, K. Sugasawa, E. Weterings, N.G. Jaspers, and J.H. Hoeijmakers. 1998. DNA-binding polarity of human replication protein A positions nucleases in nucleotide excision repair. *Genes Dev.* 12:2598–2609. doi:10.1101/gad.12.16.2598

Dinant, C., M.S. Luijsterburg, T. Höfer, G. von Bornstaedt, W. Vermeulen, A.B. Houtsmuller, and R. van Driel. 2009. Assembly of multiprotein complexes that control genome function. *J. Cell Biol.* 185:21–26. doi:10.1083/jcb.200811080

Dip, R., U. Camenisch, and H. Naegeli. 2004. Mechanisms of DNA damage recognition and strand discrimination in human nucleotide excision repair. *DNA Repair (Amst.).* 3:1409–1423. doi:10.1016/j.dnarep.2004.05.005

Dundr, M., U. Hoffmann-Rohrer, Q. Hu, I. Grummt, L.I. Rothblum, R.D. Phair, and T. Misteli. 2002. A kinetic framework for a mammalian RNA polymerase in vivo. *Science.* 298:1623–1626. doi:10.1126/science.1076164

Essers, J., A.F. Theil, C. Baldeyron, W.A. van Cappellen, A.B. Houtsmuller, R. Kanaar, and W. Vermeulen. 2005. Nuclear dynamics of PCNA in DNA replication and repair. *Mol. Cell. Biol.* 25:9350–9359. doi:10.1128/MCB.25.21.9350-9359.2005

Evans, E., J.G. Moggs, J.R. Hwang, J.M. Egly, and R.D. Wood. 1997. Mechanism of open complex and dual incision formation by human nucleotide excision repair factors. *EMBO J.* 16:6559–6573. doi:10.1093/emboj/16.21.6559

Giglia-Mari, G., C. Miquel, A.F. Theil, P.O. Mari, D. Hoogstraten, J.M. Ng, C. Dinant, J.H. Hoeijmakers, and W. Vermeulen. 2006. Dynamic interaction of TTDA with TFIIH is stabilized by nucleotide excision repair in living cells. *PLoS Biol.* 4:e156. doi:10.1371/journal.pbio.0040156

Gillet, L.C., and O.D. Schärer. 2006. Molecular mechanisms of mammalian global genome nucleotide excision repair. *Chem. Rev.* 106:253–276. doi:10.1021/cr040483f

Gorski, S.A., S.K. Snyder, S. John, I. Grummt, and T. Misteli. 2008. Modulation of RNA polymerase assembly dynamics in transcriptional regulation. *Mol. Cell.* 30:486–497. doi:10.1016/j.molcel.2008.04.021

Green, C.M., and G. Almouzni. 2003. Local action of the chromatin assembly factor CAF-1 at sites of nucleotide excision repair in vivo. *EMBO J.* 22:5163–5174. doi:10.1093/emboj/cdg478

Hall, H., J. Gurský, A. Nicodemou, I. Rybanská, E. Kimlíčková, and M. Pirsel. 2006. Characterization of ERCC3 mutations in the Chinese hamster ovary 27-1, UV24 and MMC-2 cell lines. *Mutat. Res.* 593:177–186.

Henricksen, L.A., C.B. Umbricht, and M.S. Wold. 1994. Recombinant replication protein A: expression, complex formation, and functional characterization. *J. Biol. Chem.* 269:11121–11132.

Hey, T., G. Lipps, K. Sugasawa, S. Iwai, F. Hanaoka, and G. Krauss. 2002. The XPC-HR23B complex displays high affinity and specificity for damaged DNA in a true-equilibrium fluorescence assay. *Biochemistry.* 41:6583–6587. doi:10.1021/bi012202t

Hoeijmakers, J.H. 2001. Genome maintenance mechanisms for preventing cancer. *Nature.* 411:366–374. doi:10.1038/35077232

Hoogstraten, D., A.L. Nigg, H. Heath, L.H. Mullenders, R. van Driel, J.H. Hoeijmakers, W. Vermeulen, and A.B. Houtsmuller. 2002. Rapid switching of TFIIH between RNA polymerase I and II transcription and DNA repair in vivo. *Mol. Cell.* 10:1163–1174. doi:10.1016/S1097-2765(02)00709-8

Hoogstraten, D., S. Bergink, J.M. Ng, V.H. Verbiest, M.S. Luijsterburg, B. Geverts, A. Raams, C. Dinant, J.H. Hoeijmakers, W. Vermeulen, and A.B. Houtsmuller. 2008. Versatile DNA damage detection by the global genome nucleotide excision repair protein XPC. *J. Cell Sci.* 121:2850–2859. doi:10.1242/jcs.031708

Hopfield, J.J. 1974. Kinetic proofreading: a new mechanism for reducing errors in biosynthetic processes requiring high specificity. *Proc. Natl. Acad. Sci. USA.* 71:4135–4139. doi:10.1073/pnas.71.10.4135

Houtsmuller, A.B., S. Rademakers, A.L. Nigg, D. Hoogstraten, J.H. Hoeijmakers, and W. Vermeulen. 1999. Action of DNA repair endonuclease ERCC1/XPF in living cells. *Science.* 284:958–961. doi:10.1126/science.284.5416.958

Karpova, T.S., M.J. Kim, C. Spriet, K. Nalley, T.J. Stasevich, Z. Kherrouche, L. Heliot, and J.G. McNally. 2008. Concurrent fast and slow cycling of a transcriptional activator at an endogenous promoter. *Science.* 319:466–469. doi:10.1126/science.1150559

Kaufmann, W.K., and S.J. Wilson. 1990. DNA repair endonuclease activity during synchronous growth of diploid human fibroblasts. *Mutat. Res.* 236:107–117.

Kesseler, K.J., W.K. Kaufmann, J.T. Reardon, T.C. Elston, and A. Sancar. 2007. A mathematical model for human nucleotide excision repair: damage recognition by random order assembly and kinetic proofreading. *J. Theor. Biol.* 249:361–375. doi:10.1016/j.jtbi.2007.07.025

Kimura, H., and P.R. Cook. 2001. Kinetics of core histones in living human cells: little exchange of H3 and H4 and some rapid exchange of H2B. *J. Cell Biol.* 153:1341–1353. doi:10.1083/jcb.153.7.1341

Kremers, G.J., J. Goedhart, E.B. van Munster, and T.W. Gadella Jr. 2006. Cyan and yellow super fluorescent proteins with improved brightness, protein folding, and FRET Förster radius. *Biochemistry.* 45:6570–6580. doi:10.1021/bi0516273

Kremers, G.J., K.L. Hazelwood, C.S. Murphy, M.W. Davidson, and D.W. Piston. 2009. Photoconversion in orange and red fluorescent proteins. *Nat. Methods.* 6:355–358. doi:10.1038/nmeth.1319

Kunkel, T.A., and K. Bebenek. 2000. DNA replication fidelity. *Annu. Rev. Biochem.* 69:497–529. doi:10.1146/annurev.biochem.69.1.497

Luijsterburg, M.S., J. Goedhart, J. Moser, H. Kool, B. Geverts, A.B. Houtsmuller, L.H. Mullenders, W. Vermeulen, and R. van Driel. 2007. Dynamic in vivo interaction of DDB2 E3 ubiquitin ligase with UV-damaged DNA is independent of damage-recognition protein XPC. *J. Cell Sci.* 120:2706–2716. doi:10.1242/jcs.008367

MacInnes, M.A., J.A. Dickson, R.R. Hernandez, D. Learmonth, G.Y. Lin, J.S. Mudgett, M.S. Park, S. Schauer, R.J. Reynolds, G.F. Strniste, et al. 1993. Human ERCC5 cDNA-cosmid complementation for excision repair and bipartite amino acid domains conserved with RAD proteins of *Saccharomyces cerevisiae* and *Schizosaccharomyces pombe. Mol. Cell. Biol.* 13:6393–6402.

Maillard, O., S. Solyom, and H. Naegeli. 2007. An aromatic sensor with aversion to damaged strands confers versatility to DNA repair. *PLoS Biol.* 5:e79. doi:10.1371/journal.pbio.0050079

Michelman-Ribeiro, A., D. Mazza, T. Rosales, T.J. Stasevich, H. Boukari, V. Rishi, C. Vinson, J.R. Knutson, and J.G. McNally. 2009. Direct measurement of association and dissociation rates of DNA binding in live cells by fluorescence correlation spectroscopy. *Biophys. J.* 97:337–346. doi:10.1016/j.bpj.2009.04.027

Min, J.H., and N.P. Pavletich. 2007. Recognition of DNA damage by the Rad4 nucleotide excision repair protein. *Nature.* 449:570–575. doi:10.1038/nature06155

Misteli, T. 2007. Beyond the sequence: cellular organization of genome function. *Cell.* 128:787–800. doi:10.1016/j.cell.2007.01.028

Mocquet, V., J.P. Lainé, T. Riedl, Z. Yajin, M.Y. Lee, and J.M. Egly. 2008. Sequential recruitment of the repair factors during NER: the role of XPG in initiating the resynthesis step. *EMBO J.* 27:155–167. doi:10.1038/sj.emboj.7601948

Moné, M.J., M. Volker, O. Nikaido, L.H. Mullenders, A.A. van Zeeland, P.J. Verschure, E.M. Manders, and R. van Driel. 2001. Local UV-induced DNA damage in cell nuclei results in local transcription inhibition. *EMBO Rep.* 2:1013–1017. doi:10.1093/embo-reports/kve224

Moné, M.J., T. Bernas, C. Dinant, F.A. Goedvree, E.M. Manders, M. Volker, A.B. Houtsmuller, J.H. Hoeijmakers, W. Vermeulen, and R. van Driel. 2004. In vivo dynamics of chromatin-associated complex formation in mammalian nucleotide excision repair. *Proc. Natl. Acad. Sci. USA.* 101:15933–15937. doi:10.1073/pnas.0403664101

Moser, J., M. Volker, H. Kool, S. Alekseev, H. Vrieling, A. Yasui, A.A. van Zeeland, and L.H. Mullenders. 2005. The UV-damaged DNA binding protein mediates efficient targeting of the nucleotide excision repair complex to UV-induced photo lesions. *DNA Repair (Amst.).* 4:571–582. doi:10.1016/j.dnarep.2005.01.001

Moser, J., H. Kool, I. Giakzidis, K. Caldecott, L.H. Mullenders, and M.I. Fousteri. 2007. Sealing of chromosomal DNA nicks during nucleotide excision repair requires XRCC1 and DNA ligase III alpha in a cell-cycle-specific manner. *Mol. Cell.* 27:311–323. doi:10.1016/j.molcel.2007.06.014

Mu, D., D.S. Hsu, and A. Sancar. 1996. Reaction mechanism of human DNA repair excision nuclease. *J. Biol. Chem.* 271:8285–8294. doi:10.1074/jbc.271.32.19451

Mullenders, L.H., A.A. van Zeeland, and A.T. Natarajan. 1987. The localization of ultraviolet-induced excision repair in the nucleus and the distribution of repair events in higher order chromatin loops in mammalian cells. *J. Cell Sci. Suppl.* 6:243–262.

Nishi, R., S. Alekseev, C. Dinant, D. Hoogstraten, A.B. Houtsmuller, J.H. Hoeijmakers, W. Vermeulen, F. Hanaoka, and K. Sugasawa. 2009. UV-DDB-dependent regulation of nucleotide excision repair kinetics in living cells. *DNA Repair (Amst.).* 8:767–776. doi:10.1016/j.dnarep.2009.02.004

O'Donovan, A., A.A. Davies, J.G. Moggs, S.C. West, and R.D. Wood. 1994. XPG endonuclease makes the 3′ incision in human DNA nucleotide excision repair. *Nature.* 371:432–435. doi:10.1038/371432a0

Park, C.J., and B.S. Choi. 2006. The protein shuffle. Sequential interactions among components of the human nucleotide excision repair pathway. *FEBS J.* 273:1600–1608. doi:10.1111/j.1742-4658.2006.05189.x

Perdiz, D., P. Grof, M. Mezzina, O. Nikaido, E. Moustacchi, and E. Sage. 2000. Distribution and repair of bipyrimidine photoproducts in solar UV-irradiated mammalian cells. Possible role of Dewar photoproducts in solar mutagenesis. *J. Biol. Chem.* 275:26732–26742.

Politi, A., M.J. Moné, A.B. Houtsmuller, D. Hoogstraten, W. Vermeulen, R. Heinrich, and R. van Driel. 2005. Mathematical modeling of nucleotide excision repair reveals efficiency of sequential assembly strategies. *Mol. Cell.* 19:679–690. doi:10.1016/j.molcel.2005.06.036

Polo, S.E., D. Roche, and G. Almouzni. 2006. New histone incorporation marks sites of UV repair in human cells. *Cell.* 127:481–493. doi:10.1016/j.cell.2006.08.049

Press, W., S. Teukolsky, W. Vetterling, and B. Flannery. 2007. Numerical Recipes: The Art of Scientific Computing. Third edition. Cambridge University Press, Cambridge/New York. 1235 pp.

Rademakers, S., M. Volker, D. Hoogstraten, A.L. Nigg, M.J. Moné, A.A. Van Zeeland, J.H. Hoeijmakers, A.B. Houtsmuller, and W. Vermeulen. 2003. *Xeroderma pigmentosum* group A protein loads as a separate factor onto DNA lesions. *Mol. Cell. Biol.* 23:5755–5767. doi:10.1128/MCB.23.16.5755-5767.2003

Riedl, T., F. Hanaoka, and J.M. Egly. 2003. The comings and goings of nucleotide excision repair factors on damaged DNA. *EMBO J.* 22:5293–5303. doi:10.1093/emboj/cdg489

Satokata, I., K. Tanaka, N. Miura, M. Narita, T. Mimaki, Y. Satoh, S. Kondo, and Y. Okada. 1992. Three nonsense mutations responsible for group A *xeroderma pigmentosum. Mutat. Res.* 273:193–202.

Schaeffer, L., R. Roy, S. Humbert, V. Moncollin, W. Vermeulen, J.H. Hoeijmakers, P. Chambon, and J.M. Egly. 1993. DNA repair helicase: a component of BTF2 (TFIIH) basic transcription factor. *Science.* 260:58–63. doi:10.1126/science.8465201

Shaner, N.C., R.E. Campbell, P.A. Steinbach, B.N. Giepmans, A.E. Palmer, and R.Y. Tsien. 2004. Improved monomeric red, orange and yellow fluorescent proteins derived from *Discosoma sp.* red fluorescent protein. *Nat. Biotechnol.* 22:1567–1572. doi:10.1038/nbt1037

Shivji, K.K., M.K. Kenny, and R.D. Wood. 1992. Proliferating cell nuclear antigen is required for DNA excision repair. *Cell.* 69:367–374. doi:10.1016/0092-8674(92)90416-A

Shivji, M.K., V.N. Podust, U. Hübscher, and R.D. Wood. 1995. Nucleotide excision repair DNA synthesis by DNA polymerase epsilon in the presence of PCNA, RFC, and RPA. *Biochemistry.* 34:5011–5017. doi:10.1021/bi00015a012

Sijbers, A.M., W.L. de Laat, R.R. Ariza, M. Biggerstaff, Y.F. Wei, J.G. Moggs, K.C. Carter, B.K. Shell, E. Evans, M.C. de Jong, et al. 1996. *Xeroderma pigmentosum* group F caused by a defect in a structure-specific DNA repair endonuclease. *Cell.* 86:811–822. doi:10.1016/S0092-8674(00)80155-5

Smith, C.A., and D.S. Okumoto. 1984. Nature of DNA repair synthesis resistant to inhibitors of polymerase alpha in human cells. *Biochemistry.* 23:1383–1391. doi:10.1021/bi00302a008

Sugasawa, K., J.M. Ng, C. Masutani, S. Iwai, P.J. van der Spek, A.P. Eker, F. Hanaoka, D. Bootsma, and J.H. Hoeijmakers. 1998. *Xeroderma pigmentosum* group C protein complex is the initiator of global genome nucleotide excision repair. *Mol. Cell.* 2:223–232. doi:10.1016/S1097-2765(00)80132-X

Sugasawa, K., J. Akagi, R. Nishi, S. Iwai, and F. Hanaoka. 2009. Two-step recognition of DNA damage for mammalian nucleotide excision repair: Directional binding of the XPC complex and DNA strand scanning. *Mol. Cell.* 36:642–653. doi:10.1016/j.molcel.2009.09.035

Tapias, A., J. Auriol, D. Forget, J.H. Enzlin, O.D. Schärer, F. Coin, B. Coulombe, and J.M. Egly. 2004. Ordered conformational changes in damaged DNA induced by nucleotide excision repair factors. *J. Biol. Chem.* 279:19074–19083. doi:10.1074/jbc.M312611200

Tsodikov, O.V., D. Ivanov, B. Orelli, L. Staresincic, I. Shoshani, R. Oberman, O.D. Schärer, G. Wagner, and T. Ellenberger. 2007. Structural basis for the recruitment of ERCC1-XPF to nucleotide excision repair complexes by XPA. *EMBO J.* 26:4768–4776. doi:10.1038/sj.emboj.7601894

van Attikum, H., and S.M. Gasser. 2009. Crosstalk between histone modifications during the DNA damage response. *Trends Cell Biol.* 19:207–217. doi:10.1016/j.tcb.2009.03.001

van den Boom, V., E. Citterio, D. Hoogstraten, A. Zotter, J.M. Egly, W.A. van Cappellen, J.H. Hoeijmakers, A.B. Houtsmuller, and W. Vermeulen. 2004. DNA damage stabilizes interaction of CSB with the transcription elongation machinery. *J. Cell Biol.* 166:27–36. doi:10.1083/jcb.200401056

van Duin, M., J. de Wit, H. Odijk, A. Westerveld, A. Yasui, M.H. Koken, J.H. Hoeijmakers, and D. Bootsma. 1986. Molecular characterization of the human excision repair gene ERCC-1: cDNA cloning and amino acid homology with the yeast DNA repair gene RAD10. *Cell.* 44:913–923. doi:10.1016/0092-8674(86)90014-0

van Hoffen, A., J. Venema, R. Meschini, A.A. van Zeeland, and L.H. Mullenders. 1995. Transcription-coupled repair removes both cyclobutane pyrimidine dimers and 6-4 photoproducts with equal efficiency and in a sequential way from transcribed DNA in *xeroderma pigmentosum* group C fibroblasts. *EMBO J.* 14:360–367.

Vermeulen, W., R.J. Scott, S. Rodgers, H.J. Müller, J. Cole, C.F. Arlett, W.J. Kleijer, D. Bootsma, J.H. Hoeijmakers, and G. Weeda. 1994. Clinical heterogeneity within *xeroderma pigmentosum* associated with mutations in the DNA repair and transcription gene ERCC3. *Am. J. Hum. Genet.* 54:191–200.

Villani, G., and N. Tanguy Le Gac. 2000. Interactions of DNA helicases with damaged DNA: possible biological consequences. *J. Biol. Chem.* 275:33185–33188. doi:10.1074/jbc.R000011200

Volker, M., M.J. Moné, P. Karmakar, A. van Hoffen, W. Schul, W. Vermeulen, J.H. Hoeijmakers, R. van Driel, A.A. van Zeeland, and L.H. Mullenders. 2001. Sequential assembly of the nucleotide excision repair factors in vivo. *Mol. Cell.* 8:213–224. doi:10.1016/S1097-2765(01)00281-7

Wakasugi, M., and A. Sancar. 1999. Order of assembly of human DNA repair excision nuclease. *J. Biol. Chem.* 274:18759–18768. doi:10.1074/jbc.274.26.18759

Yagi, T., J. Tatsumi-Miyajima, M. Sato, K.H. Kraemer, and H. Takebe. 1991. Analysis of point mutations in an ultraviolet-irradiated shuttle vector plasmid propagated in cells from Japanese *xeroderma pigmentosum* patients in complementation groups A and F. *Cancer Res.* 51:3177–3182.

Ye, N., M.S. Bianchi, N.O. Bianchi, and G.P. Holmquist. 1999. Adaptive enhancement and kinetics of nucleotide excision repair in humans. *Mutat. Res.* 435:43–61.

Yokoi, M., C. Masutani, T. Maekawa, K. Sugasawa, Y. Ohkuma, and F. Hanaoka. 2000. The *xeroderma pigmentosum* group C protein complex XPC-HR23B plays an important role in the recruitment of transcription factor IIH to damaged DNA. *J. Biol. Chem.* 275:9870–9875. doi:10.1074/jbc.275.13.9870

Zotter, A., M.S. Luijsterburg, D.O. Warmerdam, S. Ibrahim, A. Nigg, W.A. van Cappellen, J.H. Hoeijmakers, R. van Driel, W. Vermeulen, and A.B. Houtsmuller. 2006. Recruitment of the nucleotide excision repair endonuclease XPG to sites of UV-induced dna damage depends on functional TFIIH. *Mol. Cell. Biol.* 26:8868–8879. doi:10.1128/MCB.00695-06